Title

Expansion of Pathogenic Cardiac Macrophages in Immune Checkpoint Inhibitor Myocarditis.

Journal

Circulation, 149(1)

Authors

Ma, Pan
Liu, Jing
Qin, Juan
et al.

Publication Date

2024-01-02

DOI

10.1161/CIRCULATIONAHA.122.062551

Peer reviewed

HHS Public Access

Author manuscript

Circulation. Author manuscript; available in PMC 2024 August 14.

Published in final edited form as:

Circulation. 2024 January 02; 149(1): 48–66. doi:10.1161/CIRCULATIONAHA.122.062551.

Expansion of Pathogenic Cardiac Macrophages in Immune Checkpoint Inhibitor Myocarditis

Pan Ma, PhD,
Cardiovascular Division, Department of Medicine, Washington University School of Medicine, St Louis, MO

Jing Liu, PhD,
Cardiovascular Division, Department of Medicine, Washington University School of Medicine, St Louis, MO

Juan Qin, PhD,
Washington University School of Medicine, St Louis, MO. Division of Cardiology, Department of Medicine, University of California San Francisco

Lulu Lai, MS,
Department of Pathology and Immunology, Washington University School of Medicine, St Louis, MO

Gyu Seong Heo, PhD,
Mallinckrodt Institute of Radiology, Washington University School of Medicine, St Louis, MO

Hannah Luehmann, MS,
Mallinckrodt Institute of Radiology, Washington University School of Medicine, St Louis, MO

Deborah Sultan, PhD,
Mallinckrodt Institute of Radiology, Washington University School of Medicine, St Louis, MO

Andrea Bredemeyer, PhD,
Cardiovascular Division, Department of Medicine, Washington University School of Medicine, St Louis, MO

Geetika Bajapa, PhD,
Cardiovascular Division, Department of Medicine, Washington University School of Medicine, St Louis, MO

Guoshuai Feng, PhD,

Correspondence to: Kory J. Lavine, MD, PhD, Division of Cardiology, Department of Medicine, Washington University School of Medicine, 660 S Euclid, Campus Box 8086, St Louis, MO 63110, klavine@wustl.edu; or Javid Moslehi, MD, Division of Cardiology, Department of Medicine, University of California San Francisco, 555 Mission Bay Blvd South, Rm 252G, UCSF Box 3120, San Francisco, CA 94158, javid.moslehi@ucsf.edu.

Disclosures

J.M. has served on advisory boards for Bristol-Myers Squibb, Takeda, AstraZeneca, Myovant, Kurome Therapeutics, Kiniksa Pharmaceuticals, Daiichi Sankyo, CRC Oncology, BeiGene, Prelude Therapeutics, TransThera Sciences, and Cytokinetics. The other authors report no conflicts.

Supplemental Material is available at https://www.ahajournals.org/doi/suppl/10.1161/CIRCULATIONAHA.122.062551.

Cardiovascular Division, Department of Medicine, Washington University School of Medicine, St Louis, MO

Jesus Jimenez, MD, PhD,
Cardiovascular Division, Department of Medicine, Washington University School of Medicine, St Louis, MO

Ruijun He, MS,
Cardiovascular Division, Department of Medicine, Washington University School of Medicine, St Louis, MO

Antanisha Parks, BS,
Cardiovascular Division, Department of Medicine, Washington University School of Medicine, St Louis, MO

Junedh Amrute, BS,
Cardiovascular Division, Department of Medicine, Washington University School of Medicine, St Louis, MO

Ana Villanueva, MD,
Department of Pathology and Immunology, Washington University School of Medicine, St Louis, MO

Yongjian Liu, PhD,
Mallinckrodt Institute of Radiology, Washington University School of Medicine, St Louis, MO

Chieh-Yu Lin, MD, PhD,
Department of Pathology and Immunology, Washington University School of Medicine, St Louis, MO

Matthias Mack, MD,
Department of Internal Medicine II – Nephrology, Universitatsklinikum Regensburg Klinik und Poliklinik Innere Medizin II, Regensburg, Germany

Kaushik Amancherla, MD,
Department of Medicine, Vanderbilt University Medical Center, Nashville, TN

Javid Moslehi, MD,
Washington University School of Medicine, St Louis, MO. Division of Cardiology, Department of Medicine, University of California San Francisco

Kory J. Lavine, MD, PhD
Cardiovascular Division, Department of Medicine, Washington University School of Medicine, St Louis, MO; Department of Pathology and Immunology, Washington University School of Medicine, St Louis, MO

Abstract

BACKGROUND: Immune checkpoint inhibitors (ICIs), antibodies targeting PD-1 (programmed cell death protein 1)/PD-L1 (programmed death-ligand 1) or CTLA4 (cytotoxic T-lymphocyte–associated protein 4), have revolutionized cancer management but are associated with devastating immune-related adverse events including myocarditis. The main risk factor for ICI myocarditis

is the use of combination PD-1 and CTLA4 inhibition. ICI myocarditis is often fulminant and is pathologically characterized by myocardial infiltration of T lymphocytes and macrophages. Although much has been learned about the role of T-cells in ICI myocarditis, little is understood about the identity, transcriptional diversity, and functions of infiltrating macrophages.

METHODS: We used an established murine ICI myocarditis model (*Ctla4*$^{+/-}$*Pdcd1*$^{-/-}$ mice) to explore the cardiac immune landscape using single-cell RNA-sequencing, immunostaining, flow cytometry, in situ RNA hybridization, molecular imaging, and antibody neutralization studies.

RESULTS: We observed marked increases in CCR2 (C-C chemokine receptor type 2)$^{+}$ monocyte-derived macrophages and CD8^{+} T-cells in this model. The macrophage compartment was heterogeneous and displayed marked enrichment in an inflammatory CCR2^{+} subpopulation highly expressing *Cxcl9* (chemokine [C-X-C motif] ligand 9), *Cxcl10* (chemokine [C-X-C motif] ligand 10), *Gbp2b* (interferon-induced guanylate-binding protein 2b), and *Fcgr4* (Fc receptor, IgG, low affinity IV) that originated from CCR2^{+} monocytes. It is important that a similar macrophage population expressing *CXCL9, CXCL10,* and CD16α (human homologue of mouse FcgR4) was expanded in patients with ICI myocarditis. In silico prediction of cell-cell communication suggested interactions between T-cells and *Cxcl9*$^{+}$*Cxcl10*$^{+}$ macrophages via IFN-γ (interferon gamma) and CXCR3 (CXC chemokine receptor 3) signaling pathways. Depleting CD8^{+} T-cells or macrophages and blockade of IFN-γ signaling blunted the expansion of *Cxcl9*$^{+}$*Cxcl10*$^{+}$ macrophages in the heart and attenuated myocarditis, suggesting that this interaction was necessary for disease pathogenesis.

CONCLUSIONS: These data demonstrate that ICI myocarditis is associated with the expansion of a specific population of IFN-γ–induced inflammatory macrophages and suggest the possibility that IFN-γ blockade may be considered as a treatment option for this devastating condition.

Keywords

CXCL9 chemokine; cytotoxic T lymphocyte-associated antigen 4-immunoglobulin; IFN-gamma; macrophages; myocarditis; programmed cell death protein 1; T-cells

Immune checkpoint inhibitors (ICIs) have revolutionized cancer therapy. Remarkable improvements in clinical response rates, tumor-free and overall survival have led to the widespread use of these agents across various malignancies.[1-3] ICIs are now combined where 2 separate immune checkpoints, eg, PD-1 (programmed cell death protein 1)/PD-L1 (programmed death-ligand 1) and CTLA4 (cytotoxic T-lymphocyte–associated protein 4) or LAG3 (lymphocyte activating 3), are inhibited with demonstration of greater antitumor efficacy. However, ICIs, especially when used in combination, are associated with a wide spectrum of immune-related adverse events that can affect any organ.[4,5] Although infrequent, myocarditis is the most serious immune-related adverse event with high mortality despite corticosteroid therapy. ICI myocarditis is characterized by T-cell and macrophage infiltration with associated cardiomyocyte death. Patients often present with electrocardiographic disturbances including conduction block and ventricular arrhythmias; 50% of patients have a normal systolic cardiac function.[6,7] Combined use of PD-1 and CTLA4 inhibitors is the major risk factor for myocarditis. Higher frequency of myocarditis was reported in patients treated with combination treatment (1.22%) compared with PD-1/PD-L1 or CTLA4 inhibitors alone (0.54%).[8] Previous studies addressing ICI myocarditis

pathogenes is primarily focused on T-cells.[9-12] However, less is known about macrophage populations in ICI myocarditis and potential communication between immune cell types, such as T-cells and macrophages.

Under steady state conditions, the heart contains predominantly macrophages with smaller populations of T-cells, B-cells, and dendritic cells (DCs).[13] Cardiac macrophages represent a heterogeneous population of cells that can be divided into 2 major subsets with differing origins and functions: cardiac resident $CCR2^{-}$ macrophages and monocyte-derived $CCR2^{+}$ macrophages.[14-16] Among these subsets, $CCR2^{+}$ macrophages display the greatest inflammatory potential and contribute to myocardial inflammation and heart failure pathogenesis. $CCR2^{+}$ macrophages generate numerous inflammatory mediators (cytokines, chemokines, oxidative products) and function as antigen-presenting cells. In experimental acute autoimmune myocarditis, CCR2 silencing attenuates disease.[17,18]

It is well recognized that activated T-cells communicate with macrophages as a component of the host immune response in the setting of infection and autoimmunity.[19] Nevertheless, how macrophages contribute to ICI myocarditis and to what degree macrophage–T-cell cross-talk modulates this process are not clear. Immune checkpoint therapies including PD-1 and CTLA4 inhibitors boost T-cell responses and promote abundant cytokine production.[20] Within the context of ICI myocarditis, interactions between activated T-cells and cardiac macrophages may drive myocardial inflammation and contribute to disease pathogenesis. This possibility remains to be explored.

Here, we dissected the cardiac immune landscape of ICI myocarditis using an established mouse model (*Ctla4*$^{+/-}$*Pdcd1*$^{-/-}$ mice) by employing immunostaining, flow cytometry, in situ RNA hybridization, single-cell RNA-sequencing, molecular imaging and antibody neutralization studies. We observed evidence of $CD8^{+}$ T-cell activation and expansion of an inflammatory $CCR2^{+}$ monocyte-derived macrophage population that displayed a transcriptional signature characterized by *Cxcl9, Cxcl10, Gbp2b,* and *Fcgr4* expression that originated from $CCR2^{+}$ monocytes. A similar population of macrophages expressing *CXCL9, CXCL10,* and CD16α (human homologue of mouse FcgR4) were expanded in patients with ICI myocarditis to a greater degree than those with chronic heart failure and lymphocytic myocarditis. Informatic prediction of cell-cell communication suggested that T-cells regulate the expansion of *Cxcl9*$^{+}$*Cxcl10*$^{+}$ macrophages via IFN-γ signaling and implied a positive feedback loop between these cell types mediated by *CXCL9, CXCL10,* and CXCR3 signaling. Consistent with this prediction, depleting $CD8^{+}$T-cells or macrophages and blockade of IFN-γ signaling blunted the expansion of *Cxcl9*$^{+}$*Cxcl10*$^{+}$ macrophages in the heart and prolonged survival. Collectively, these data demonstrate that ICI myocarditis is associated with the expansion of a specific population of IFN-γ induced inflammatory macrophages and suggest the possibility that IFN-γ blockade may serve as a potential intervention strategy for this devastating condition.

METHODS

Mouse Strains

All animal studies were performed in compliance with guidelines set forth by the National Institutes of Health Office of Laboratory Animal Welfare and approved by the Washington University institutional animal care and use committee. Animals were housed in a controlled environment with a 12-hour light-dark cycle, with free access to water and a standard chow diet. *Ctla4*$^{+/+}$*Pdcd1*$^{-/-}$, *Ctla4*$^{+/-}$*Pdcd1*$^{-/-}$ mice were maintained as previously described.[8] All mice were genotyped according to established protocols. Female mice were primarily used in the experiments.

Study Approval and Human Pathological Specimens

This study was approved by the Institutional Review Board of Washington University (Study No. 201104172) in St Louis. Hematoxylin and eosin–stained slides were reviewed by cardiovascular pathologists to confirm the diagnosis. Clinical information of human samples is included in Table S1.

Statistical Analyses

Normal distribution of quantification results was tested by Shapiro-Wilk test. Significance of the quantification results was tested by the Mann-Whitney test or Welch's *t* test or Student's *t* test using Prism 9.0 (GraphPad Software, San Diego, CA). *P* value <0.05 was considered as significant.

Data and Codes Availability

All the codes used in the article are deposited in GitHub (pma22wustl/Expansion-of-Pathogenic-Cardiac-Macrophages-in-Immune-Checkpoint-Inhibitor-Myocarditis [github.com]). Other data are available on reasonable request from the lead contact. The single-cell raw expression matrices and raw sequence files that support the findings of this study are available on the Gene Expression Omnibus (GSE227437, GSE230192). Published RNA-sequencing (RNA-seq) data of male mice that support the findings of this study are available on the Gene Expression Omnibus (GSE225099). Published RNA-seq data of patients with ICI-associated myocarditis are available in the EBI (European Bioinformatics Institute) ArrayExpress Database, accession No. E-MTAB-8867.[21]

RESULTS

Accumulation of CCR2^{+} Macrophages in a Mouse Model of ICI Myocarditis

To dissect the cardiac immune landscape of ICI myocarditis, we used a previously validated mouse model of this condition whereby haploinsufficiency in *Ctla4* in the background of PD-1 deficiency (*Pdcd1*$^{-/-}$) results in sudden cardiac death and pathological characteristics consistent with ICI myocarditis. Clinical features include electrocardiographic disturbances with relatively preserved cardiac function consistent with human disease. Immune infiltration is limited to a few tissues including the heart, with higher prevalence of disease in female mice.[8] As such, given the variability of presentation with myocarditis,

female mice were primarily used in this study. Consistent with previous reports,[12] we detected robust immune cell accumulation in the hearts of *Ctla4*$^{+/-}$*Pdcd1*$^{-/-}$ mice with increased abundance of T-cells (CD8$^+$ > CD4$^+$) (Figure S1A) and CD68$^+$ macrophages (Figure 1A) compared with wild-type (WT) mice. *Ctla4*$^{+/+}$*Pdcd1*$^{-/-}$ mice displayed an intermediate phenotype. Flow cytometry demonstrated increased macrophage, CD8$^+$ T-cell, and CD4$^+$ T-cell abundance in *Ctla4*$^{+/-}$*Pdcd1*$^{-/-}$ hearts compared with *Ctla4*$^{+/+}$*Pdcd1*$^{-/-}$ hearts (Figure 1B). Natural killer cells (NK-cells) and B-cells were not affected (Figure S1B). Further phenotyping of the monocyte/macrophage compartment revealed increased frequency of LY-6C (lymphocyte antigen 6C)^{high} monocytes and CCR2$^+$ macrophages in *Ctla4*$^{+/-}$*Pdcd1*$^{-/-}$ hearts compared with *Ctla4*$^{+/+}$*Pdcd1*$^{-/-}$ hearts (Figure 1C). Using in situ hybridization, we detected robust *Ccr2* mRNA expression in *Cd68*$^+$ macrophages in *Ctla4*$^{+/-}$*Pdcd1*$^{-/-}$ hearts (Figure 1D). These findings were confirmed by CCR2 targeted positron emission tomography/computed tomography imaging as previously demonstrated.[22] ^{68}Ga-DOTA-ECL1i positron emission tomography/computed tomography revealed increased uptake in the hearts of *Ctla4*$^{+/-}$*Pdcd1*$^{-/-}$ *mice* compared with WT and *Ctla4*$^{+/+}$*Pdcd1*$^{-/-}$ hearts (Figure 1E). Collectively, these findings reveal that ICI myocarditis is associated with the accumulation of CCR2$^+$ macrophages.

Expansion of a Unique Population of CCR2$^+$ Macrophages in a Mouse Model of ICI Myocarditis

To explore the cardiac immune landscape of ICI myocarditis, we performed scRNA-seq of heart tissue from control (*Ctla4*$^{+/+}$*Pdcd1*$^{-/-}$, n=4) and ICI myocarditis (*Ctla4*$^{+/-}$*Pdcd1*$^{-/-}$, n=10) mice. We constructed 5 libraries (control: L1, L2; disease: L3, L4, L5) from DRAQ5$^+$DAPI$^-$ cells purified from pooled enzymatically digested hearts by fluorescence-activated cell sorting (Figure S2A). After quality control filters were applied (Figure S2B), unsupervised clustering revealed 8 major cell types (Figure 2A, Figure S2C). Cell identities were annotated using cell type–specific markers (Figure S2D). The major immune cell clusters identified were myeloid cells and T/NK-cells. Smaller populations of B-cells and neutrophils were also detected. Further subclustering of myeloid cells based on their transcriptomic features demonstrated 5 myeloid subpopulations (Figure 2B and 2C). In addition to monocytes and DCs, 3 groups of macrophages (defined by the expression of canonical macrophage genes such as *Cd68, C1qa, C1qb, C1qc*; Figure S3) were identified. Analysis of individual marker genes (Figure 2D) and marker gene scores (Figure 2E) demonstrated that cardiac resident macrophages (*Cd163*$^+$ resident Mac) expressed canonical markers of tissue resident macrophages including *Cd163, Lyve1* (lymphatic vessel endothelial hyaluronan receptor 1), *Folr2* (folate receptor beta), and *Cbr2* (carbonyl reductase 2).[23,24] The other 2 macrophage subpopulations, *Cxcl9*$^+$*Cxcl10*$^+$ Mac and *Nlrp3* (NLR family pyrin domain containing 3)$^+$ Mac, each expressed *Ccr2* and were differentiated by specific marker gene signatures (*Cxcl9*$^+$*Cxcl10*$^+$ Mac: *Cxcl9, Cxcl10* and *Nlrp3*$^+$ Mac: *Nlrp3, Ccl4* [chemokine (C-C motif) ligand 4], *Cd14*). Among these populations, the abundance of *Cxcl9*$^+$*Cxcl10*$^+$ macrophages increased in *Ctla4*$^{+/-}$*Pdcd1*$^{-/-}$ hearts compared with *Ctla4*$^{+/-}$*Pdcd1*$^{-/-}$ hearts (Figure 2C). We further generated scRNA-seq data from WT mouse hearts (n=6) (Figure S4A) and mapped the dataset onto the original object consisting of *Ctla4*$^{+/+}$*Pdcd1*$^{-/-}$ (n=4) and *Ctla4*$^{+/-}$ *Pdcd1*$^{-/-}$ (n=10) myeloid cells (Figure S4B). WT myeloid cells (640 cells) predominantly mapped to 3 subclusters: *Cd163* resident Mac, DCs,

and monocytes, with majority of prediction scores >0.75 (Figure S4A, S4C, and S4D). In contrast, few cells mapped to *Cxcl9 Cxcl10* Mac cluster. Low predication scores were observed among WT cells for *Cxcl9 Cxcl10* Mac subset (Figure S4A and S4D). These data indicate that *Cxcl9*$^{+}$*Cxcl10*$^{+}$ macrophages cannot be confidently identified within the query (WT) dataset (Figure S4C and S4D). Consistently, a limited number of cells expressing *Cxcl9* were identified in WT myeloid dataset (Figure S4E).

Cxcl9^{+}*Cxcl10*$^{+}$ Macrophages Exhibited an Activated Phenotype in ICI Myocarditis Mouse Hearts

To further investigate differences between myeloid cells found within *Ctla4*$^{+/+}$*Pdcd1*$^{-/-}$ and *Ctla4*$^{+/-}$*Pdcd1*$^{-/-}$ hearts, we performed a differential gene expression analysis using our scRNA-seq dataset. *Cxcl9, Cxcl10, Gbp2b, Ccl8, Ccl5, Fcgr4, Ly6a, Lgals3,* and *AW112010* were upregulated in myeloid cells from *Ctla4*$^{+/+}$*Pdcd1*$^{-/-}$ mice (Figure 3A and Figure S5). The top 10 upregulated genes in *Ctla4*$^{+/-}$*Pdcd1*$^{-/-}$ mice were exclusively expressed in the *Cxcl9*$^{+}$*Cxcl10*$^{+}$ macrophage subcluster (Figure 3B) suggesting that the expansion and activation of *Cxcl9*$^{+}$*Cxcl10*$^{+}$ macrophages represented the predominate difference in myeloid cells between experimental groups. Further validation of expression of *Cxcl9, Cxcl10, Gbp2b*, *Ccl8*, and *Fcgr4* mRNA expression using RT-PCR revealed striking increases in the myocardium of *Ctla4*$^{-/-}$ *Pdcd1*$^{-/-}$ compared to *Ctla4*$^{+/+}$*Pdcd1*$^{-/-}$ hearts (Figure 3C). *In situ* hybridization revealed increased absolute abundance frequency of *Cxcl9*$^{+}$*Ccr2*$^{+}$ and *Cxcl10*$^{+}$*Ccr2*$^{+}$ macrophages in *Ctla4*$^{+/-}$*Pdcd1*$^{-/-}$ hearts compared with wide type and *Ctla4*$^{+/+}$*Pdcd1*$^{-/-}$ hearts. The majority of *Cxcl9*$^{+}$ and *Cxcl10*$^{+}$ cells co-expressed *Ccr2* and were identified as macrophages in *Ctla4*$^{+/-}$*Pdcd1*$^{-/-}$ hearts (Figure 3D). Flow cytometry showed increased FCGR4 protein expression on *Ctla4*$^{+/-}$*Pdcd1*$^{-/-}$ macrophages (Figure 3E). To identify *Cxcl9*$^{+}$*Cxcl10*$^{+}$ macrophages subsets among CCR2^{+} macrophages by flow cytometry, we examined the expression of FCGR4 (a surface protein). We observed significantly increased frequency of CCR2^{+}FCGR4^{high} macrophages in *Ctla4*$^{+/-}$*Pdcd1*$^{-/-}$ hearts compared with *Ctla4*$^{+/+}$*Pdcd1*$^{-/-}$ hearts (Figure S18).

Gene ontology enrichment pathway analysis using genes upregulated in *Ctla4*$^{+/-}$*Pdcd1*$^{-/-}$ mice indicated that response to IFN-γ signaling, cytokine-mediated signaling, myeloid cell migration, and antigen presentation were among the most affected pathways (Figure 3F). Each of these pathways localized to the *Cxcl9*$^{+}$*Cxcl10*$^{+}$ macrophage cluster (Figure 3G). These data suggest that *Cxcl9*$^{+}$*Cxcl10*$^{+}$ macrophages in ICI myocarditis may represent an activated population with enhanced potential for migration, inflammatory cytokine/chemokine production, IFN-γ signaling, and antigen presentation. We also observed a similar phenotype in male *Ctla4*$^{+/-}$*Pdcd1*$^{-/-}$ hearts demonstrated by increased CD68^{+} macrophage accumulation and expansion of *Cxcl9*$^{+}$*Cxcl10*$^{+}$ macrophages compared with male *Ctla4*$^{+/+}$*Pdcd1*$^{-/-}$ hearts (Figure S6). In addition, *Cxcl9*$^{+}$*Cxcl10*$^{+}$ macrophages exhibited distinct phenotypes compared with *Nlrp3*$^{+}$ macrophages or *Cd163*$^{+}$ resident macrophages (Figure S7). Compared with *Cxcl9*$^{+}$*Cxcl10*$^{+}$ macrophages, *Nlrp3*$^{+}$ macrophages exhibited enrichment for genes implicated in the response to LPS, regulation of IL-1β production, and stromal cell proliferation. *Cd163*$^{+}$ resident macrophages displayed enrichment for pathways involved in regulating epithelial cell proliferation and response to stress.

Furthermore, gene regulatory network analysis using the SCENIC (single-cell regulatory network inference and clustering) pipeline, which identifies modules of transcription factors coexpressed with their target genes, referred to as regulons,[25] revealed that activated *Cxcl9*$^{+}$*Cxcl10*$^{+}$ macrophage in ICI myocarditis showed a unique and specific transcriptional regulatory network. Downstream transcription factors of IFN-γ including STAT1 (signal transducer and activator of transcription 1) and IRF7 (interferon regulatory factor 7) were enriched in activated *Cxcl9*$^{+}$*Cxcl10*$^{+}$ macrophage (Figure S8A). RNA transcripts of Stat1 and Irf7 were present in the *Cxcl9*$^{+}$*Cxcl10*$^{+}$ macrophage subcluster (Figure S8B). TF (transcription factor) regulatory network analysis predicted several downstream genes regulated by these TFs in the *Cxcl9*$^{+}$*Cxcl10*$^{+}$ macrophage subcluster, including *Cxcl9, Cxcl10, Gbp2,* and *Fcgr4* (Figure S8C). To validate this, we analyzed the expression and phosphorylated state of STAT1 protein in hearts from *Ctla4*$^{+/+}$*Pdcd1*$^{-/-}$ and *Ctla4*$^{+/-}$*Pdcd1*$^{-/-}$ mice (Figure S8D). Compared with control *Ctla4*$^{+/+}$*Pdcd1*$^{-/-}$ mice, *Ctla4*$^{+/-}$*Pdcd1*$^{-/-}$ mice exhibited significant enhanced expression and phosphorylation levels of STAT1, indicating the activation of IFN-γ signaling pathway. In vitro, we also found that inhibition of STAT1 activation using a JAK1/2 inhibitor, ruxolitinib, significantly suppressed IFN-γ induced *Cxcl9* expression in bone marrow derived macrophages (Figure S8E). Knockdown of *Stat1* expression in bone marrow derived macrophages by small interfering RNA significantly reduced IFN-γ–induced *Cxcl9* expression (Figure S8F). These findings indicate an important role for IFN-γ–STAT1 signaling in the emergence of *Cxcl9*$^{+}$*Cxcl10*$^{+}$ macrophages.

Cxcl9^{+}*Cxcl10*$^{+}$ Macrophages Originated From CCR2^{+} Monocytes

To gain further insights into the relationships between myeloid subclusters, we performed trajectory analysis using Palantir.[26] We specified the starting point as monocytes. Calculation of pseudotime values suggested that *Cd163*$^{+}$ macrophages, *Cxcl9*$^{+}$*Cxcl10*$^{+}$ macrophages, *Nlrp3*$^{+}$ macrophages, and DCs represented differentiated cell states. Ascertainment of differentiation potential (entropy) values indicated that *Cxcl9*$^{+}$*Cxcl10*$^{+}$ macrophages displayed the lowest level of cell plasticity, highlighting that this may represent a highly specialized cell state (Figure 4A, 4B, and 4D). We then calculated terminal state probabilities for DCs, *Cd163*$^{+}$ macrophages, and *Cxcl9*$^{+}$*Cxcl10*$^{+}$ macrophages differentiating from monocytes. DCs and *Cd163*$^{+}$ macrophage terminal state probabilities were largely restricted to cells within their respective clusters. In contrast, high terminal state probabilities for the *Cxcl9*$^{+}$*Cxcl10*$^{+}$ macrophage state was evident, suggesting a development relationship from monocytes (Figure 4C and 4D). Compared with control mice, *Cxcl9*$^{+}$*Cxcl10*$^{+}$ macrophages from *Ctla4*$^{+/+}$*Pdcd1*$^{-/-}$ mice exhibited lower entropy and higher terminal state probability values, suggesting these macrophages in diseased mice are more differentiated and functionally activated (Figure 4D). In addition, we used a neutralizing CCR2 antibody (MC-21) to inhibit monocyte mobilization in *Ctla4*$^{+/-}$*Pdcd1*$^{-/-}$ mice. MC-21 blocks the interaction between CCR2 and CCL2, which prevents the recruitment of CCR2^{+} monocytes to sites of inflammation and results in reduction of macrophages derived from recruited CCR2^{+} monocytes.[27,28] Consistent with the findings of our trajectory analysis, MC-21 antibody treatment reduced the accumulation of CD68^{+} macrophages (Figure S9) and the abundance of *Cxcl9*$^{+}$*Cxcl10*$^{+}$ macrophages (Figure 4E and 4F), and decreased the frequency of CCR2^{+}FCGR4^{high} macrophages (Figure S18).

Through lineage tracing of recruited monocytes, we have confirmed that MC-21 displays similar properties in the heart (Figure S10). These findings demonstrate the dependence of *Cxcl9*$^{+}$*Cxcl10*$^{+}$ macrophages on monocytes.

CXCL9^{+}*CXCL10*$^{+}$ Macrophages in Clinical Cases of ICI Myocarditis

We next examined whether macrophages expressing *CXCL9, CXCL10,* and CD16α (human homologue of mouse FcgR4) were present with the myocardium of patients with ICI myocarditis. In situ hybridization revealed robust expression of *CXCL9* and *CXCL10* mRNA in interstitial cells within the myocardium of patients with biopsy-confirmed ICI myocarditis. In contrast, rare cells expressing *CXCL9* and *CXCL10* mRNA were detected in healthy donors, and subjects with dilated cardiomyopathy, ischemic cardiomyopathy, and lymphocytic myocarditis (Figure 5A). Immunostaining further revealed expansion of CD16α^{+} macrophages in subjects with ICI myocarditis. Consistent with our mouse scRNA-seq data, CD16α^{+} macrophages expressed CCR2 in ICI myocarditis samples. Few CD16α^{+} macrophages were observed in dilated cardiomyopathy, ischemic cardiomyopathy, and lymphocytic myocarditis (Figure 5B). In situ hybridization and immunostaining performed on consecutive sections obtained from ICI myocarditis specimens revealed colocation of *CXCL9* and *CXCL10* mRNA with CD68, CD16α, and CCR2 protein (Figure S11). These findings confirm the existence of *CXCL9*$^{+}$*CXCL10*$^{+}$ macrophages in human ICI myocarditis.

T-cells Are the Major Source of IFN-γ in ICI Myocarditis Mouse Hearts

Pathway analysis indicated that *Cxcl9*$^{+}$*Cxcl10*$^{+}$ macrophages express an IFN-γ activation signature, suggesting that cardiac IFN-γ signaling may regulate the differentiation or activity of this macrophage population. Consistent with this possibility, we detected increased expression of *Ifng* mRNA in *Ctla4*$^{+/-}$*Pdcd1*$^{-/-}$ hearts compared with *Ctla4*$^{+/+}$*Pdcd1*$^{-/-}$ control hearts (Figure 6A). To identify the cellular source of IFN-γ, we leveraged our scRNA-seq dataset and observed robust expression of *Ifng* mRNA in the T/NK-cell cluster (Figure 6B). High-resolution clustering of T-cells and NK-cells identified 4 major subclusters including CD8^{+} T-cells, CD4^{+} T-cells, NK-cells, and naïve T-cells with differing transcriptional signatures (Figure S12A). *Ifng* mRNA was readily expressed in CD4^{+} and CD8^{+} T-cells (Figure 6C). Intracellular flow cytometry confirmed that CD4^{+} and CD8^{+} T-cells produced increased amounts of IFN-γ in *Ctla4*$^{+/-}$*Pdcd1*$^{-/-}$ hearts compared with controls. Macrophages and NK-cells produced low amounts of IFN-γ. Among T-cell populations, CD8^{+} T-cells displayed the greatest increase in IFN-γ expression (Figure 6D).

Detailed examination of T-cell subclusters revealed expansion of CD8^{+} T-cells in *Ctla4*$^{+/-}$*Pdcd1*$^{-/-}$ hearts compared with *Ctla4*$^{+/+}$*Pdcd1*$^{-/-}$ control hearts (Figure 6E). Differential expression analysis identified robust transcriptional differences between experimental groups. The top 10 genes upregulated in *Ctla4*$^{+/-}$*Pdcd1*$^{-/-}$ T/NK-cells (*Nrn1* [neuritin 1], *Prf1* [perforin-1], *Icos* [inducible T-cell costimulator], *Lars2* [probable leucyl-tRNA synthetase], *Cd8a, Cd5, Stat1, Klrd1* [killer cell lectin like receptor D1], *Btg1* [B-cell translocation gene 1 protein], *Lag3*) mapped to CD8^{+} T-cells (Figure 6F). Gene ontology and Kyoto Encyclopedia of Genes and Genomes pathway analysis implicated enhanced T-cell activation, T-cell differentiation and cytokine-cytokine receptor signaling as putative

markers of T-cell activation in *Ctla4*$^{+/-}$*Pdcd1*$^{-/-}$ hearts (Figure 6G, Figure S12B and S12C). These data highlight the putative pathological role of CD8^{+} T-cells in our mouse model of ICI myocarditis.

IFN-γ and CXCR3 Signaling Are Predicted to Mediate Cross-Talk Between *Cxcl9*$^{+}$*Cxcl10*$^{+}$ Macrophages and T-Cells

To investigate cross-talk between macrophages and T-cells in ICI myocarditis, we applied CellChat to infer cell-cell communication. We identified several possible ligand-receptor interactions. Predicted signals outgoing from CD4^{+} T-cells and CD8^{+} T-cells included IFN-II, MIF (macrophage migration inhibitory factor pathway), and FASL (Fas ligand). Each of these signals was predicted to be received by *Cxcl9*$^{+}$*Cxcl10*$^{+}$ macrophages. CXCL ligands and CD137 were predicted to signal from *Cxcl9*$^{+}$*Cxcl10*$^{+}$ macrophages to T-cells (Figure S13).

Among these pathways, we focused on IFN-II and CXCL signaling given their enrichment in *Cxcl9*$^{+}$*Cxcl10*$^{+}$ macrophages and CD8^{+} T-cells, respectively. We first examined *Ifng, Ifngr1,* and *Ifngr2* mRNA expression in macrophages and T-cells. *Ifng* was selectively expressed in CD4^{+} and CD8^{+} T-cells. *Ifngr1* was expressed in all macrophages and T-cells, and *Ifngr2* was exclusively expressed in *Cxcl9*$^{+}$*Cxcl10*$^{+}$ macrophages (Figure 7A). CellChat pathway network analysis predicted that CD4^{+} T-cells and CD8^{+} T-cells were the primary ligand sources and that *Cxcl9*$^{+}$*Cxcl10*$^{+}$ macrophages served as the receivers of IFN-γ signaling (Figure 7B and 7C). CD8^{+} T-cells demonstrated a higher communication probability compared with CD4^{+} T-cells (Figure 7D).

Reciprocal signaling from *Cxcl9*$^{+}$*Cxcl10*$^{+}$ macrophages to T-cells was further explored using CellChat, which predicted that these cell types interact through CXCL signaling. *Cxcl9*$^{+}$*Cxcl10*$^{+}$ macrophages were predicted to serve as the source of CXCL ligands that signaled to CD4^{+} T-cells and CD8^{+} T-cells through the CXCR3 receptor (Figure 7E through 7G). CXCR3 is reported to activate mitogen-activated protein kinases and phosphoinositide 3-kinase/protein kinase B (PI3K/AKT) pathways leading to activation, differentiation, and recruitment of T-cells.[29,30] CellChat also identified CXCL16 (chemokine [C-X-C motif] ligand 16)–CXCR6 (CXC chemokine receptor 6) signaling as a second pathway that may mediate interactions between macrophages and T-cells (Figure S14).

To evaluate the predicted interaction between CD8^{+} T-cells and *Cxcl9*$^{+}$*Cxcl10*$^{+}$ macrophages, we depleted CD8^{+} T-cells in *Ctla4*$^{+/-}$*Pdcd1*$^{-/-}$ mice with anti-CD8 antibody beginning at 4 weeks of life (Figure S15A). CD8 depletion reduced *Cxcl9*$^{+}$*Cxcl10*$^{+}$ macrophages in the heart, indicated by decreased cardiac *Cxcl9* and *Cxcl10* expression (Figure S15B, Figure 7H) and reduced frequency of CCR2^{+}FCGR4^{high} macrophages (Figure S18). We also leveraged the bulk RNA-seq dataset from 9 human ICI-associated myocarditis biopsy samples[21] and observed a positive correlation between *CD8A* and *CXCL9/10/FCGR3A* (low-affinity immunoglobulin gamma Fc region receptor III-A) expression (Figure S16). Collectively, these findings support a role for CD8^{+} T-cells in the expansion and activation of *Cxcl9*$^{+}$*Cxcl10*$^{+}$ macrophages.

IFN-γ Blockade and Macrophage Depletion Reduced *Cxcl9*$^{+}$*Cxcl10*$^{+}$ Macrophages and Prolonged Survival of *Ctla4*$^{+/-}$*Pdcd1*$^{-/-}$ Mice

To examine the causal role of IFN-γ signaling in the activation and expansion of *Cxcl9*$^{+}$*Cxcl10*$^{+}$ macrophages and effect on ICI myocarditis, we examined the effects of blocking IFN-γ signaling. *Ctla4*$^{+/-}$*Pdcd1*$^{-/-}$ mice were treated with either isotype control or IFN-γ neutralization antibody (Clone, R46A2) beginning at 3 weeks of life. IFN-γ blockade significantly prolonged the survival of *Ctla4*$^{+/-}$*Pdcd1*$^{-/-}$ mice (Figure 8A). Previous studies have demonstrated that these mice die from myocarditis and arrhythmic events.[8] In situ hybridization revealed markedly diminished cardiac *Cxcl9* and *Cxcl10* expression in anti–IFN-γ antibody–treated *Ctla4*$^{+/-}$*Pdcd1*$^{-/-}$ mice compared with isotype control–treated *Ctla4*$^{+/-}$*Pdcd1*$^{-/-}$ mice, implying a reduction in *Cxcl9*$^{+}$*Cxcl10*$^{+}$ macrophages (Figure 8B). IFN-γ blockade reduced the frequency of CCR2^{+}FCGR4^{high} macrophages in the heart, consistent with a reduction in *Cxcl9*$^{+}$*Cxcl10*$^{+}$ macrophages (Figure S18). Within the CD64^{+} compartment, we observed that CCR2^{+} cells consisted of CCR2^{+}MHC (major histocompatibility complex)^{high} macrophages and CCR2^{+}MHC^{low} monocytes/macrophages (CCR2^{+} monocytes and differentiating macrophages[16]). We observed a reduced percentage and absolute number of CCR2^{+}MHC^{low} monocytes/macrophages in the heart after 3 weeks of IFN-γ blockade. We did not detect any differences in the abundance of CCR2^{+}MHC^{high} macrophages in the heart. These data indicate that IFN-γ reshapes CCR2^{+}MHCII^{high} macrophages towards an activated *Cxcl9*$^{+}$*Cxcl10*$^{+}$ phenotype (*Cxcl9*$^{+}$*Cxcl10*$^{+}$*Ccr2*$^{+}$macrophages) and influences the recruitment of CCR2^{+} monocytes and their differentiation into macrophages (Figure S17A). It is important to note that we did not detect significant changes in T-cell abundance and phenotype across CD4^{+} and CD8^{+} subsets between control and anti–IFN-γ–treated groups, arguing against a direct effect on T-cells at this time point (Figure S17B through S17D). These findings indicate that inhibition of IFN-γ signaling prevented the expansion of activated *Cxcl9*$^{+}$*Cxcl10*$^{+}$ macrophages and suppressed the progression of ICI myocarditis. It is important to note that temporary blockade of IFN-γ signaling does not interfere with the therapeutic effects of conventional chemotherapy.[31,32]

To further study the role of *Cxcl9*$^{+}$*Cxcl10*$^{+}$ macrophages in ICI myocarditis, we depleted macrophages in the heart by administrating anti-CSF1R antibody in Ctla*4*$^{+/-}$*Pdcd1*$^{-/-}$ mice beginning at 3 weeks of age (Figure 8E). Anti-CSF1R treatment significantly prolonged the survival of *Ctla4*$^{+/-}$*Pdcd1*$^{-/-}$ mice (Figure 8C) and markedly reduced the number of *Cxcl9*$^{+}$*Cxcl10*$^{+}$ macrophages. These findings are consistent with what we observed in the IFN-γ blockade experiments (Figure 8D) corroborating the functional importance of macrophages in ICI myocarditis.

DISCUSSION

ICI myocarditis is a serious manifestation of ICI-induced toxicity. Histological analysis of myocardial specimens from patients with ICI myocarditis revealed immune infiltrates composed of CD4^{+} T-cells, CD8^{+} T-cells, and macrophages[4,8,9,33] Substantial effort has focused on elucidating mechanisms of T-cell infiltration and expansion within the heart,[9-12] including the recognition of clonal populations of T-cells that recognize antigens

co-expressed in the tumor and the heart.[6] Markedly less is known about macrophage populations in ICI myocarditis. Within this context, the transcriptomic features of macrophages, their inherent heterogeneity, and their effect on disease progression remain incompletely explored.

Here, we used an established genetic ICI myocarditis model (*Ctla4*$^{+/-}$*Pdcd1*$^{-/-}$ mice), which recapitulates clinical features seen in subjects with fulminant ICI myocarditis.[8] Using a compilation of technologies (scRNA-seq, immunostaining, in situ hybridization, flow cytometry, antibody neutralization, and molecular imaging), we demonstrated that ICI myocarditis is associated with the expansion of a population of CCR2^{+} macrophages (*Cxcl9*$^{+}$*Cxcl10*$^{+}$ macrophages) that expressed a transcriptional signature indicative of enhanced IFN-γ activation, cytokine generation, myeloid cell migration, and antigen presentation. A similar population of macrophages was identified in human cases of ICI myocarditis, which expanded in this pathological entity. *Cxcl9*$^{+}$*Cxcl10*$^{+}$ macrophages originated from CCR2^{+} monocytes. Mechanistically, *Cxcl9*$^{+}$*Cxcl10*$^{+}$ macrophages were predicted to be specified by activated T-cells through IFN-γ signaling and participate in a positive feedback loop with T-cells through CXCR3 signaling. Depleting CD8^{+} T-cells or CD64^{+} cells and blocking IFN-γ signaling led to reductions in *Cxcl9*$^{+}$*Cxcl10*$^{+}$ macrophages and improved survival in our mouse model of ICI myocarditis. These data provide support for the possibility that IFN-γ signaling may be considered as a potential target for the treatment of ICI-associated myocarditis.

CXCL9 and CXCL10 are robustly expressed by macrophages that emerge in the setting of ICI myocarditis (*Ctla4*$^{+/-}$*Pdcd1*$^{-/-}$ mouse model and human ICI myocarditis specimens). CXCL9-expressing macrophages are similarly found in ICI-treated patients and those who developed ICI colitis.[34,35] Trajectory analysis predicted that *Cxcl9*$^{+}$*Cxcl10*$^{+}$ macrophages were derived from recruited monocytes, which was validated by selective depletion of Ly6C^{hi} monocytes. This finding is consistent with the repeated observation that inflammatory macrophage populations are derived from monocytes that infiltrate the heart after injury.[16,36,37]In silico analysis further indicated that IFN-γ stimulation orchestrated the differentiation of infiltrating monocytes or monocyte-derived macrophages into *Cxcl9*$^{+}$*Cxcl10*$^{+}$ macrophages. The functional importance of IFN-γ signaling and *Cxcl9*$^{+}$*Cxcl10*$^{+}$ macrophages was validated through our neutralizing antibody studies. Anecdotal clinical studies have recently reported that CTLA4-fusion protein abatacept combined with the Janus kinase inhibitor ruxolitinib, which targets IFN-γ/JAK2/STAT1 signaling, decreased cardiovascular death among patients with ICI myocarditis.[38] Understanding the contribution of IFN-γ signaling to the specification and expansion of *Cxcl9*$^{+}$*Cxcl10*$^{+}$ macrophages and the function of these cells in ICI myocarditis and related pathologies are of considerable interest.

Cxcl9^{+}*Cxcl10*$^{+}$ macrophages may contribute to ICI myocarditis pathogenesis through several distinct mechanisms including enhancing T-cell responses, innate immune cell recruitment, and directly aggravating local tissue damage. *Cxcl9*$^{+}$*Cxcl10*$^{+}$ macrophages express several inflammatory mediators involved in T-cell migration and T-cell receptor signaling, highlighting the possibility that they are primed to augment T-cell activation. Consistent with our findings, patients with ICI myocarditis display enhanced expression

of CXCR3 on T-cells, particularly memory $CD8^+$ T-cells.[34,39] $CD8^+$ T-cells serve as the predominant cardiac T-cell subset in ICI myocarditis, display an activated phenotype, and produce IFN-γ. Using the same mouse model of ICI myocarditis, it was observed that $CD8^+$ T-cells are clonally expanded, target alpha-myosin as a MHC-I restricted autoantigen, and are required for disease pathogenesis.[12] Similarly, Zhu and colleagues observed clonally expanded activated Temra (T-effector memory cells re-expressing CD45RA) $CD8^+$ T-cells along with increased monocytes and macrophages in the hearts of MRL/*Pdcd1*$^{-/-}$ mice with spontaneous myocarditis.[39] Informatic prediction of cell-cell communication suggested that $CD8^+$ T-cells signal to *Cxcl9*$^+$*Cxcl10*$^+$ macrophages by secreting IFN-γ. This analysis also predicted a reciprocal feedback loop where *Cxcl9*$^+$*Cxcl10*$^+$ macrophages communicated with $CD8^+$ T-cells through CXCL16/CXCR6 signaling and with $CD4^+$ and $CD8^+$ T-cells through CXCL9/CXCL10-CXCR3 signaling. *Cxcl9*$^+$*Cxcl10*$^+$ macrophages may stimulate the recruitment and activation of $CD8^+$ T-cells and potentially trigger cytotoxic responses against cardiomyocytes, which warrants further investigation.

In addition to regulating T-cell chemotaxis, *Cxcl9*$^+$*Cxcl10*$^+$ macrophages may also participate in promoting peripheral monocyte and neutrophil recruitment. *Cxcl9*$^+$*Cxcl10*$^+$ macrophages represent a subset of $CCR2^+$ macrophages and express chemokines that regulate peripheral leukocyte migration and chemotaxis as predicted by pathway analysis. After cardiac injury, $CCR2^+$ monocytes are recruited to the heart by $CCR2^+$ macrophages through an MYD88 (myeloid differentiation primary response 88)–dependent mechanism by the production of chemokines including CCL2/MCP1 (monocyte chemoattractant protein 1) and CCL7/MCP3 (monocyte chemoattractant protein 3).[16] This raises the possibility that *Cxcl9*$^+$*Cxcl10*$^+$ macrophages further enhance myocardial inflammation by recruiting additional peripheral immune cells.

Cxcl9$^+$*Cxcl10*$^+$ macrophages may also contribute to cardiomyocyte injury and cell death by activating effector T-cells or inducing antibody-dependent cytotoxicity (ADCC) and phagocytosis.[40] De novo autoantibodies (including to cardiac antigens) have been reported to develop in ~20% of patients with ICI-treated melanoma.[41,42] In the presence of anticardiac autoantibodies, *Cxcl9*$^+$*Cxcl10*$^+$ macrophages are ideally positioned to participate in ADCC and target cell phagocytosis.[40] IFN signaling enhances ADCC function of macrophages,[43] and FcgR4 (human CD16α) represents an essential surface receptor to initiate the ADCC.[40]

In considering strategies to treat ICI myocarditis, it is important to recognize that selected therapeutic targets should ideally not interfere with ongoing or established tumor control. At present, conflicting data exist about whether IFN-γ signaling is essential for maintaining the therapeutic response to ICIs. Administration of ICIs leads to enhanced IFN-γ, CXCL9, and CXCL10 production in the tumor microenvironment, which facilitates entry of lymphocytes that eliminate tumor cells.[44] Intriguingly, IFN-γ production also promotes tumor immunoevasion[45] and participates in doxorubicin-associated cardiotoxicity.[31,32] The exact phase of requirement for IFN-γ signaling in maintaining tumor control after ICI therapy is unclear. Moving forward, it will be essential to determine how IFN-γ blockade compares with other proposed ICI myocarditis treatments including CTLA4-Ig

(abatacept),[8,46] anti-CD52 (alemtuzumab),[47] and anti-TNFα (tumor necrosis factor α) (infliximab)[48] in regards to effects on both ICI myocarditis and tumor control.

Our study is not without limitations. We acknowledge that there is no perfect animal model of ICI myocarditis and that *Ctla4*$^{+/-}$*Pdcd1*$^{-/-}$ mice may only recapitulate some aspects of the disease. We further recognize that IFN-γ blockade represents a starting point and that considerable work remains to elucidate the functions of *Cxcl9*$^{+}$*Cxcl10*$^{+}$ macrophages, dissect downstream signaling mechanisms, and define optimal therapeutic targets. Short-term treatment (3 weeks) of anti–IFN-γ did not significantly affect the abundance of CD8^{+} T-cells. It remains possible that longer-term inhibition of IFN-γ signaling may have an effect on the number of CD8^{+} T-cells. It is also plausible that anti–IFN-γ treatment affects CD8^{+} T-cell phenotypes and gene expression. This is an important possibility that will be investigated in future studies. Nonetheless, our findings advance the field by identifying a targetable population of macrophages in ICI myocarditis. In conclusion, we demonstrate that IFN-γ signaling triggers the expansion of an inflammatory population of *Cxcl9*$^{+}$*Cxcl10*$^{+}$ macrophages in ICI myocarditis that is potentially positioned to augment T-cell recruitment, T-cell activation, chemokine/cytokine production, and ADCC, and that blockade of IFN-γ signaling may be considered as a potential approach that requires further evaluation for the treatment of this devastating condition.

Supplementary Material

Refer to Web version on PubMed Central for supplementary material.

Acknowledgments

P.M., J.M., and K.J.L. conceived and designed the study and composed the article. P.M. and K.J.L. analyzed all data generated in this study. J.M., K.J.L. supervised the study. P.M., G.F., and A.V. managed the mouse colony and identified appropriate animals for each experiment. P.M., J.L., and R.H. performed flow cytometry experiments. P.M., J.L., J.Q., L.L., and J.A. performed single-cell RNA and bulk RNA-seq data analyses and figure generation. P.M. and J.Q. performed antibody-mediated depletion and neutralization studies. P.M., A.B., and G.B. prepared samples for single-cell sequencing. G.S.H., H.L., and D.S. performed CCR2 positron emission tomography/computed tomography experiments, and Y.L. analyzed the positron emission tomography/computed tomography data. M.M. provided MC-21 antibody and technical expertise in experimental design. J.M., K.A., J.J., A.P., and C.Y.L. provided clinical expertise and assistance acquiring slides from human specimens for this study.

Sources of Funding

K.J.L. is supported by the Washington University in St Louis Rheumatic Diseases Research Resource-Based Center grant (NIH P30AR073752), National Institutes of Health (R01 HL138466, R01 HL139714, R01 HL151078, R01 HL161185, R35 HL161185], Leducq Foundation Network (20CVD02), Burroughs Welcome Fund (1014782), Children's Discovery Institute of Washington University and St Louis Children's Hospital (CH-II-2015-462, CH-II-2017-628, PM-LI-2019-829), and Foundation of Barnes-Jewish Hospital (8038-88), and generous gifts from Washington University School of Medicine. J.M. is supported by National Institutes of Health grants (R01HL141466, R01HL155990, R01HL156021, R01HL160688). Y.L. is supported by National Institutes of Health grants (R35HL145212, R01HL131908, R01HL150891, R01HL153436, R01HL151685-01A1, P41EB025815). P.M. is supported by an American Heart Association Postdoctoral Fellowship (916955).

Glossary

ADCC	antibody-dependent cytotoxicity
AKT	Rho family serine/threonine protein kinase, protein kinase B

Btg1	B-cell translocation gene 1 protein
Cbr2	carbonyl reductase 2
Ccl4	chemokine (C-C motif) ligand 4
Ccl5	chemokine (C-C motif) ligand 5
Ccl8	chemokine (C-C motif) ligand 8
CCR2	C-C chemokine receptor type 2
CTLA4	cytotoxic T-lymphocyte–associated protein 4
CXCL9	chemokine (C-X-C motif) ligand 9
CXCL10	chemokine (C-X-C motif) ligand 10
CXCL16	chemokine (C-X-C motif) ligand 16
CXCR3	CXC chemokine receptor 3
CXCR6	CXC chemokine receptor 6
DC	dendritic cell
FASL	Fas ligand
FCGR3A	low-affinity immunoglobulin gamma Fc region receptor III-A
Fcgr4	Fc receptor, IgG, low affinity IV
Folr2	folate receptor beta
Gbp2b	interferon-induced guanylate-binding protein 2b
ICI	immune checkpoint inhibitor
Icos	inducible T-cell costimulator
IFN-γ	interferon gamma
Klrd1	killer cell lectin like receptor D1
Lag3	lymphocyte activating 3
Lars2	probable leucyl-tRNA synthetase
Lgals3	galectin-3
LY-6C	lymphocyte antigen 6C
Lyve1	lymphatic vessel endothelial hyaluronan receptor 1
MCP1	monocyte chemoattractant protein 1
MCP3	monocyte chemoattractant protein 3

MHC	major histocompatibility complex
MIF	macrophage migration inhibitory factor pathway
MYD88	myeloid differentiation primary response 88
NK-cell	natural killer cell
Nlrp3	NLR family pyrin domain containing 3
Nrn1	neuritin 1
PD-1	programmed cell death protein 1
PD-L1	programmed death-ligand 1
Prf1	perforin-1
RNA-seq	RNA-sequencing
SCENIC	single-cell regulatory network inference and clustering
scRNA-seq	single-cell RNA-sequencing
Stat1	signal transducer and activator of transcription 1
TF	transcription factor
TNFα	tumor necrosis factor α
WT	wild-type

REFERENCES

1. Wolchok JD, Kluger H, Callahan MK, Postow MA, Rizvi NA, Lesokhin AM, Segal NH, Ariyan CE, Gordon R-A, Reed K, et al. Nivolumab plus ipilimumab in advanced melanoma. N Engl J Med. 2013;369:122–133. doi: 10.1056/NEJMoa1302369 [PubMed: 23724867]
2. Postow MA, Chesney J, Pavlick AC, Robert C, Grossmann K, McDermott D, Linette GP, Meyer N, Giguere JK, Agarwala SS, et al. Nivolumab and ipilimumab versus ipilimumab in untreated melanoma. N Engl J Med. 2015;372:2006–2017. doi: 10.1056/NEJMoa1414428 [PubMed: 25891304]
3. Motzer RJ, Tannir NM, McDermott DF, Frontera OA, Melichar B, Choueiri TK, Plimack ER, Barthélémy P, Porta C, George S. Nivolumab plus ipilimumab versus sunitinib in advanced renal-cell carcinoma. N Engl J Med. 2018;378:1277–1290. doi: 10.1056/NEJMoa1712126 [PubMed: 29562145]
4. Heinzerling L, Ott PA, Hodi FS, Husain AN, Tajmir-Riahi A, Tawbi H, Pauschinger M, Gajewski TF, Lipson EJ, Luke JJ. Cardiotoxicity associated with CTLA4 and PD1 blocking immunotherapy. J ImmunoTher Cancer. 2016;4:1–11.
5. Varricchi G, Galdiero MR, Marone G, Criscuolo G, Triassi M, Bonaduce D, Marone G, Tocchetti CG. Cardiotoxicity of immune checkpoint inhibitors. ESMO Open. 2017;2:e000247 doi: 10.1136/esmoopen-2017-000247 [PubMed: 29104763]
6. Johnson DB, Balko JM, Compton ML, Chalkias S, Gorham J, Xu Y, Hicks M, Puzanov I, Alexander MR, Bloomer TL, et al. Fulminant myocarditis with combination immune checkpoint blockade. N Engl J Med. 2016;375:1749–1755. doi: 10.1056/NEJMoa1609214 [PubMed: 27806233]
7. Sznol M, Ferrucci PF, Hogg D, Atkins MB, Wolter P, Guidoboni M, Lebbé C, Kirkwood JM, Schachter J, Daniels GA, et al. Pooled analysis safety profile of nivolumab and ipilimumab

combination therapy in patients with advanced melanoma. J Clin Oncol. 2017;35:3815–3822. doi: 10.1200/JCO.2016.72.1167 [PubMed: 28915085]

8. Wei SC, Meijers WC, Axelrod ML, Anang N-AA, Screever EM, Wescott EC, Johnson DB, Whitley E, Lehmann L, Courand P-Y, et al. A genetic mouse model recapitulates immune checkpoint inhibitor–associated myocarditis and supports a mechanism-based therapeutic intervention. Cancer Discov. 2021;11:614–625. doi: 10.1158/2159-8290.cd-20-0856 [PubMed: 33257470]
9. Ji C, Roy MD, Golas J, Vitsky A, Ram S, Kumpf SW, Martin M, Barletta F, Meier WA, Hooper AT, et al. Myocarditis in cynomolgus monkeys following treatment with immune checkpoint inhibitors. Clin Cancer Res. 2019;25:4735–4748. doi: 10.1158/1078-0432.CCR-18-4083 [PubMed: 31085720]
10. Wang J, Okazaki I-M, Yoshida T, Chikuma S, Kato Y, Nakaki F, Hiai H, Honjo T, Okazaki T. PD-1 deficiency results in the development of fatal myocarditis in MRL mice. Int Immunol. 2010;22:443–452. doi: 10.1093/intimm/dxq026 [PubMed: 20410257]
11. Won T, Kalinoski HM, Wood MK, Hughes DM, Jaime CM, Delgado P, Talor MV, Lasrado N, Reddy J, Cihakova D. Cardiac myosin-specific autoimmune T cells contribute to immune-checkpoint-inhibitor-associated myocarditis. Cell Rep. 2022;41:111611. doi: 10.1016/j.celrep.2022.111611 [PubMed: 36351411]
12. Axelrod ML, Meijers WC, Screever EM, Qin J, Carroll MG, Sun X, Tannous E, Zhang Y, Sugiura A, Taylor BC, et al. T cells specific for alpha-myosin drive immunotherapy-related myocarditis. Nature. 2022;611:818–826. doi: 10.1038/s41586-022-05432-3 [PubMed: 36385524]
13. Swirski FK, Nahrendorf M. Cardioimmunology: the immune system in cardiac homeostasis and disease. Nat Rev Immunol. 2018;18:733–744. doi: 10.1038/s41577-018-0065-8 [PubMed: 30228378]
14. Epelman S, Lavine KJ, Randolph GJ. Origin and functions of tissue macrophages. Immunity. 2014;41:21–35. doi: 10.1016/j.immuni.2014.06.013 [PubMed: 25035951]
15. Bajpai G, Schneider C, Wong N, Bredemeyer A, Hulsmans M, Nahrendorf M, Epelman S, Kreisel D, Liu Y, Itoh A, et al. The human heart contains distinct macrophage subsets with divergent origins and functions. Nat Med. 2018;24:1234–1245. doi: 10.1038/s41591-018-0059-x [PubMed: 29892064]
16. Bajpai G, Bredemeyer A, Li W, Zaitsev K, Koenig AL, Lokshina I, Mohan J, Ivey B, Hsiao H-M, Weinheimer C, et al. Tissue resident CCR2− and CCR2+ cardiac macrophages differentially orchestrate monocyte recruitment and fate specification following myocardial injury. Circ Res. 2019;124:263–278. doi: 10.1161/CIRCRESAHA.118.314028 [PubMed: 30582448]
17. Lu H, Zong G, Zhou S, Jiang Y, Chen R, Su Z, Wu Y. Angiotensin II–C–C chemokine receptor2/5 axis-dependent monocyte/macrophage recruitment contributes to progression of experimental autoimmune myocarditis. Microbiol Immunol. 2017;61:539–546. doi: 10.1111/1348-0421.12548 [PubMed: 29052263]
18. Leuschner F, Courties G, Dutta P, Mortensen LJ, Gorbatov R, Sena B, Novobrantseva TI, Borodovsky A, Fitzgerald K, Koteliansky V, et al. Silencing of CCR2 in myocarditis. Eur Heart J. 2015;36:1478–1488. doi: 10.1093/eurheartj/ehu225 [PubMed: 24950695]
19. Guerriero JL. Macrophages: their untold story in T cell activation and function. Int Rev Cell Mol Biol. 2019;342:73–93. doi: 10.1016/bs.ircmb.2018.07001 [PubMed: 30635094]
20. Archilla-Ortega A, Domuro C, Martin-Liberal J, Muñoz P. Blockade of novel immune checkpoints and new therapeutic combinations to boost antitumor immunity. J Exp Clin Cancer Res. 2022;41:1–24. [PubMed: 34980222]
21. Finke D, Heckmann MB, Salatzki J, Riffel J, Herpel E, Heinzerling LM, Meder B, Völkers M, Müller OJ, Frey N, et al. Comparative transcriptomics of immune checkpoint inhibitor myocarditis identifies guanylate binding protein 5 and 6 dysregulation. Cancers. 2021;13:2498. doi: 10.3390/cancers13102498 [PubMed: 34065419]
22. Heo GS, Kopecky B, Sultan D, Ou M, Feng G, Bajpai G, Zhang X, Luehmann H, Detering L, Su Y, et al. Molecular imaging visualizes recruitment of inflammatory monocytes and macrophages to the injured heart. Circ Res. 2019;124:881–890. doi: 10.1161/CIRCRESAHA.118.314030 [PubMed: 30661445]
23. Moeller JB, Nielsen MJ, Reichhardt MP, Schlosser A, Sorensen GL, Nielsen O, Tornoe I, Gronlund J, Nielsen ME, Jorgensen JS, et al. CD163-L1 is an endocytic macrophage protein strongly

regulated by mediators in the inflammatory response. J Immunol. 2012;188:2399–2409. doi: 10.4049/jimmunol.1103150 [PubMed: 22279103]

24. Dick SA, Macklin JA, Nejat S, Momen A, Clemente-Casares X, Althagafi MG, Chen J, Kantores C, Hosseinzadeh S, Aronoff L, et al. Self-renewing resident cardiac macrophages limit adverse remodeling following myocardial infarction. Nat Immunol. 2019;20:29–39. doi: 10.1038/s41590-018-0272-2 [PubMed: 30538339]
25. Aibar S, González-Blas CB, Moerman T, Huynh-Thu VA, Imrichova H, Hulselmans G, Rambow F, Marine J-C, Geurts P, Aerts J, et al. SCENIC: single-cell regulatory network inference and clustering. Nat Methods. 2017;14:1083–1086. doi: 10.1038/nmeth.4463 [PubMed: 28991892]
26. Setty M, Kiseliovas V, Levine J, Gayoso A, Mazutis L, Pe'er D. Characterization of cell fate probabilities in single-cell data with Palantir. Nat Biotechnol. 2019;37:451–460. doi: 10.1038/s41587-019-0068-4 [PubMed: 30899105]
27. Mack M, Cihak J, Simonis C, Luckow B, Proudfoot AE, Plachy J, Bruhl H, Frink M, Anders HJ, Vielhauer V, et al. Expression and characterization of the chemokine receptors CCR2 and CCR5 in mice. J Immunol. 2001;166:4697–4704. doi: 10.4049/jimmunol.166.7.4697 [PubMed: 11254730]
28. Patel B, Bansal SS, Ismahil MA, Hamid T, Rokosh G, Mack M, Prabhu SD. CCR2(+) monocyte-derived infiltrating macrophages are required for adverse cardiac remodeling during pressure overload. JACC Basic Transl Sci. 2018;3:230–244. doi: 10.1016/j.jacbts.2017.12.006 [PubMed: 30062209]
29. Rabin RL, Alston MA, Sircus JC, Knollmann-Ritschel B, Moratz C, Ngo D, Farber JM. CXCR3 is induced early on the pathway of CD4+ T cell differentiation and bridges central and peripheral functions. J Immunol. 2003;171:2812–2824. doi: 10.4049/jimmunol.171.6.2812 [PubMed: 12960302]
30. Altara R, Mallat Z, Booz GW, Zouein FA. The CXCL10/CXCR3 axis and cardiac inflammation: implications for immunotherapy to treat infectious and noninfectious diseases of the heart. J Immunol Res. 2016;2016:4396368. doi: 10.1155/2016/4396368 [PubMed: 27795961]
31. Ni C, Ma P, Wang R, Lou X, Liu X, Qin Y, Xue R, Blasig I, Erben U, Qin Z. Doxorubicin-induced cardiotoxicity involves IFNγ-mediated metabolic reprogramming in cardiomyocytes. J Pathol. 2019;247:320–332. doi: 10.1002/path.5192 [PubMed: 30426505]
32. Ma P, Qin Y, Cao H, Erben U, Ni C, Qin Z. Temporary blockade of interferon-γ ameliorates doxorubicin-induced cardiotoxicity without influencing the anti-tumor effect. Biomed Pharmacother. 2020;130:110587 doi: 10.1016/j.biopha.2020.110587 [PubMed: 32763819]
33. Weinmann SC, Pisetsky DS. Mechanisms of immune-related adverse events during the treatment of cancer with immune checkpoint inhibitors. Rheumatology. 2019;58:vii59–vii67. doi: 10.1093/rheumatology/kez308 [PubMed: 31816080]
34. Boughdad S, Latifyan S, Fenwick C, Bouchaab H, Suffiotti M, Moslehi JJ, Salem J-E, Schaefer N, Nicod-Lalonde M, Costes J, et al. 68Ga-DOTATOC PET/CT to detect immune checkpoint inhibitor-related myocarditis. J ImmunoTher Cancer. 2021;9:e003594. doi: 10.1136/jitc-2021-003594 [PubMed: 34686542]
35. Luoma AM, Suo S, Williams HL, Sharova T, Sullivan K, Manos M, Bowling P, Hodi FS, Rahma O, Sullivan RJ, et al. Molecular pathways of colon inflammation induced by cancer immunotherapy. Cell. 2020;182:655–671.e22. doi: 10.1016/j.cell.2020.06.001 [PubMed: 32603654]
36. Lavine KJ, Epelman S, Uchida K, Weber KJ, Nichols CG, Schilling JD, Ornitz DM, Randolph GJ, Mann DL. Distinct macrophage lineages contribute to disparate patterns of cardiac recovery and remodeling in the neonatal and adult heart. Proc Natl Acad Sci USA. 2014;111:16029–16034. doi: 10.1073/pnas.1406508111 [PubMed: 25349429]
37. Epelman S, Lavine KJ, Beaudin AE, Sojka DK, Carrero JA, Calderon B, Brija T, Gautier EL, Ivanov S, Satpathy AT, et al. Embryonic and adult-derived resident cardiac macrophages are maintained through distinct mechanisms at steady state and during inflammation. Immunity. 2014;40:91–104. doi: 10.1016/j.immuni.2013.11.019 [PubMed: 24439267]
38. Salem JE, Bretagne M, Abbar B, Leonard-Louis S, Ederhy S, Redheuil A, Boussouar S, Nguyen LS, Procureur A, Stein F, et al. Abatacept/ruxolitinib and screening for concomitant respiratory muscle failure to mitigate fatality of immune-checkpoint inhibitor myocarditis. Cancer Discov. 2023;13:1100–1115. doi: 10.1158/2159-8290.cd-22-1180 [PubMed: 36815259]

39. Zhu H, Galdos FX, Lee D, Waliany S, Huang YV, Ryan J, Dang K, Neal JW, Wakelee HA, Reddy SA, et al. Identification of pathogenic immune cell subsets associated with checkpoint inhibitor-induced myocarditis. Circulation. 2022;146:316–335. doi: 10.1161/CIRCULATIONAHA.121.056730 [PubMed: 35762356]
40. Braster R, O'toole T, Van Egmond M. Myeloid cells as effector cells for monoclonal antibody therapy of cancer. Methods. 2014;65:28–37. doi: 10.1016/j.ymeth.2013.06.020 [PubMed: 23811299]
41. de Moel EC, Rozeman EA, Kapiteijn EH, Verdegaal EM, Grummels A, Bakker JA, Huizinga TW, Haanen JB, Toes RE, van der Woude D. Auto-antibody development under treatment with immune-checkpoint inhibitors. Cancer Immunol Res. 2019;7:6–11. doi: 10.1158/2326-6066.cir-18-0245 [PubMed: 30425107]
42. Rikhi R, Karnuta J, Hussain M, Collier P, Funchain P, Tang WHW, Chan TA, Moudgil R. Immune checkpoint inhibitors mediated lymphocytic and giant cell myocarditis: uncovering etiological mechanisms. Front Cardiovasc Med. 2021;8:721333. doi: 10.3389/fcvm.2021.721333 [PubMed: 34434981]
43. Hokland P, Berg K. Interferon enhances the antibody-dependent cellular cytotoxicity (ADCC) of human polymorphonuclear leukocytes. J Immunol. 1981;127:1585–1588. [PubMed: 6168696]
44. Tokunaga R, Zhang W, Naseem M, Puccini A, Berger MD, Soni S, McSkane M, Baba H, Lenz H-J. CXCL9, CXCL10, CXCL11/CXCR3 axis for immune activation–a target for novel cancer therapy Cancer Treat Rev. 2018;63:40–47. doi: 10.1016/j.ctrv.2017.11.007 [PubMed: 29207310]
45. Zaidi MR. The interferon-gamma paradox in cancer. J Interferon Cytokine Res. 2019;39:30–38. doi: 10.1089/jir.2018.0087 [PubMed: 30388040]
46. Salem J-E, Allenbach Y, Vozy A, Brechot N, Johnson DB, Moslehi JJ, Kerneis M. Abatacept for severe immune checkpoint inhibitor–associated myocarditis. N Engl J Med. 2019;380:2377–2379. doi: 10.1056/nejmc1901677 [PubMed: 31189043]
47. Esfahani K, Buhlaiga N, Thébault P, Lapointe R, Johnson NA, Miller WH Jr. Alemtuzumab for immune-related myocarditis due to PD-1 therapy N Engl J Med. 2019;380:2375–2376. doi: 10.1056/NEJMc1903064 [PubMed: 31189042]
48. Michel L, Helfrich I, Hendgen-Cotta UB, Mincu R-I, Korste S, Mrotzek SM, Spomer A, Odersky A, Rischpler C, Herrmann K, et al. Targeting early stages of cardiotoxicity from anti-PD1 immune checkpoint inhibitor therapy. Eur Heart J. 2022;43:316–329. doi: 10.1093/eurheartj/ehab430 [PubMed: 34389849]
49. Jin S, Guerrero-Juarez CF, Zhang L, Chang I, Ramos R, Kuan C-H, Myung P, Plikus MV, Nie Q. Inference and analysis of cell-cell communication using CellChat. Nat Commun. 2021;12:1–20. [PubMed: 33397941]
50. Stuart T, Butler A, Hoffman P, Hafemeister C, Papalexi E, Mauck WM 3rd, Hao Y, Stoeckius M, Smibert P, Satija R. Comprehensive integration of single-cell data. Cell. 2019;177:1888–1902.e21. doi: 10.1016/j.cell.2019.05.031 [PubMed: 31178118]
51. Bruhl H, Cihak J, Plachy J, Kunz-Schughart L, Niedermeier M, Denzel A, Rodriguez Gomez M, Talke Y, Luckow B, Stangassinger M, et al. Targeting of Gr-1+,CCR2+ monocytes in collagen-induced arthritis. Arthritis Rheum. 2007;56:2975–2985. doi: 10.1002/art.22854 [PubMed: 17763443]
52. Heo GS, Bajpai G, Li W, Luehmann HP, Sultan DH, Dun H, Leuschner F, Brody SL, Gropler RJ, Kreisel D, et al. Targeted PET imaging of chemokine receptor 2–positive monocytes and macrophages in the injured heart. J Nucl Med. 2021;62:111–114. doi: 10.2967/jnumed.120.244673 [PubMed: 32444372]

Clinical Perspective

What Is New?

- We identified expansion of a subset of cardiac CCR2 (C-C chemokine receptor type 2)$^{+}$ macrophages marked by *Cxcl9* (chemokine [C-X-C motif] ligand 9) and *Cxc10* (chemokine [C-X-C motif] ligand 10) expression in mouse and human immune checkpoint inhibitor myocarditis and demonstrated their functional importance in disease pathogenesis.
- Cardiac *Cxcl9*$^{+}$*Cxc10*$^{+}$ macrophages originate from CCR2^{+} monocytes and differentiate in response to IFN-γ (interferon gamma) produced by T-cells.
- Depleting CD8^{+} T-cells and blockade of IFN-γ signaling blunted the expansion of *Cxcl9*$^{+}$*Cxcl10*$^{+}$ macrophages in the heart and attenuated myocarditis.

What Are the Clinical Implications?

- This study highlighted a critical role for a subset of IFN-γ induced inflammatory macrophages marked by *Cxcl9* and *Cxc10* expression in immune checkpoint inhibitor myocarditis.
- These data suggest that blocking IFN-γ signaling or targeting inflammatory populations of cardiac macrophages may be an effective approach to treat immune checkpoint inhibitor myocarditis.

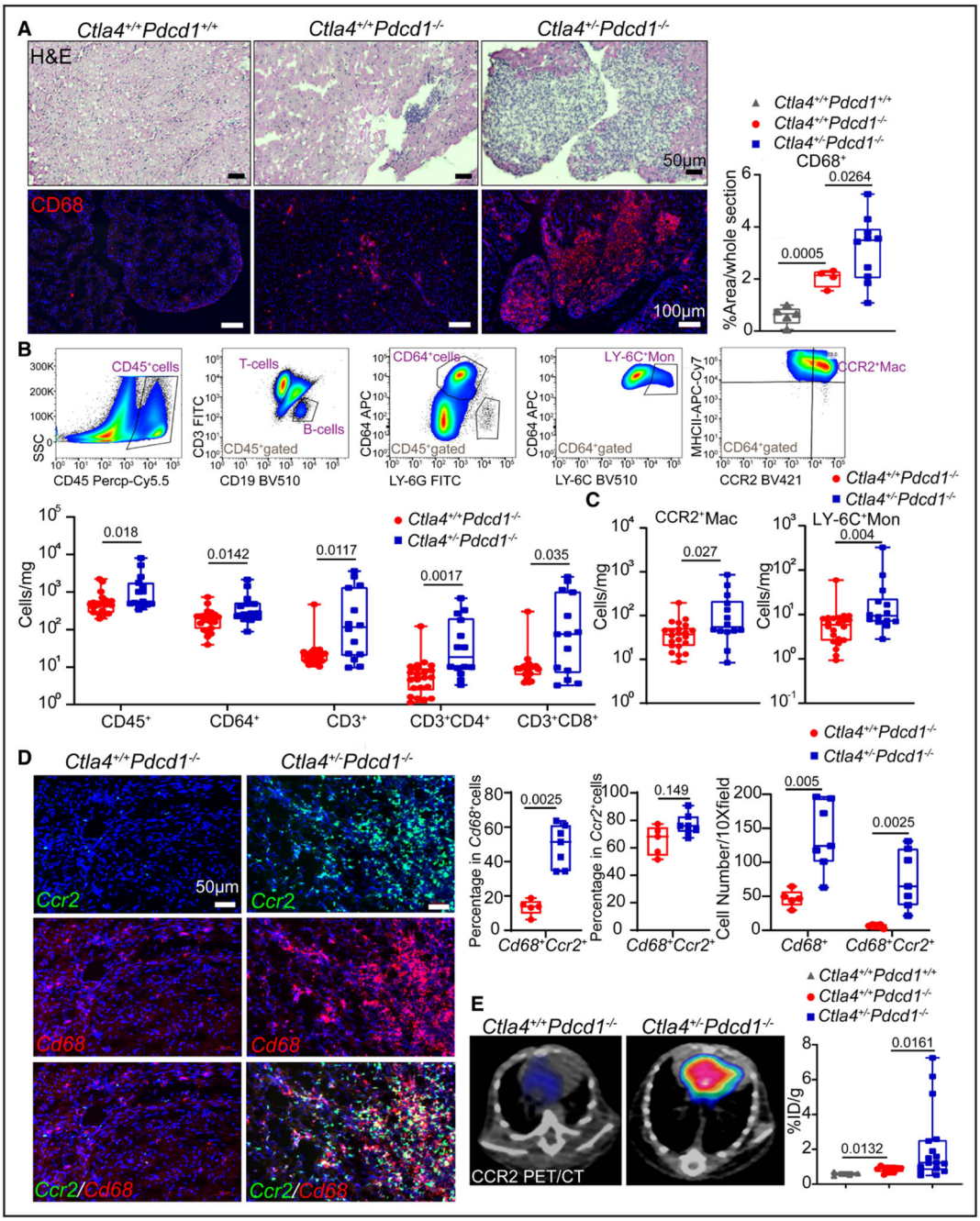

Figure 1. Accumulation of CCR2$^+$ monocytes and macrophages in *Ctla4*$^{+/-}$*Pdcd1*$^{-/-}$ mouse hearts.

A, Representative images of H&E and CD68 immunofluorescent staining (red) in wild-type (*Ctla4*$^{+/+}$*Pdcd1*$^{+/+}$), *Ctla4*$^{+/+}$*Pdcd1*$^{-/-}$, and *Ctla4*$^{+/-}$*Pdcd1*$^{-/-}$ hearts. Quantification of CD68$^+$ cells. Data collected from 2 independent experiments. *Ctla4*$^{+/+}$*Pdcd1*$^{+/+}$ (n=5), *Ctla4*$^{+/+}$*Pdcd1*$^{-/-}$ (n=4), *Ctla4*$^{+/-}$*Pdcd1*$^{-/-}$ (n=10), Welch's *t*-test, 2-tailed. Scale bar for H&E staining images, 50 μm. Scale bar for CD68 staining images, 100 μm. **B**, Quantification of CD45$^+$, CD64$^+$, CD3$^+$, CD3$^+$CD4$^+$, and CD3$^+$CD8$^+$ cells in the heart by flow cytometry.

Data collected from 4 independent experiments. *Ctla4*$^{+/+}$*Pdcd1*$^{-/-}$ (n=22), *Ctla4*$^{+/-}$*Pdcd1*$^{-/-}$ (n=14), Mann-Whitney test, 2-tailed. **C**, Quantification of CCR2^{+} macrophages and LY-6C^{high} monocytes by flow cytometry. Data collected from 4 independent experiments. *Ctla4*$^{+/+}$*Pdcd1*$^{-/-}$ (n=22), *Ctla4*$^{+/-}$*Pdcd1*$^{-/-}$ (n=14), Mann-Whitney test, 2-tailed. **D**, *Ccr2* (green) and *Cd68* (red) expression detected in *Ctla4*$^{+/+}$*Pdcd1*$^{-/-}$ and *Ctla4*$^{+/-}$*Pdcd1*$^{-/-}$ mouse hearts by RNA in situ hybridization. **Left**, Representative images, scale bar, 50 μm. **Right**, Quantification of the percentage of *Cd68*$^{+}$*Ccr2*$^{+}$cells in *Cd68*$^{+}$cells and *Ccr2*$^{+}$cells, respectively, as well as the cell numbers per 10× field. *Ctla4*$^{+/+}$*Pdcd1*$^{-/-}$ (n=5), *Ctla4*$^{+/-}$*Pdcd1*$^{-/-}$ (n=7), Mann-Whitney test, 2-tailed. **E**, In vivo cardiac CCR2 signal was detected with a CCR2 specific radiotracer, ^{64}Cu-DOTA-ECL1i, using positron emission tomography. Representative CCR2 positron emission tomography–computed tomography (PET/CT) images (**left**) and quantification of CCR2 tracer uptake (**right**). Data collected from 2 independent experiments, *Ctla4*$^{+/+}$*Pdcd1*$^{+/+}$ (n=4), *Ctla4*$^{+/+}$*Pdcd1*$^{-/-}$ (n=12), *Ctla4*$^{+/-}$*Pdcd1*$^{-/-}$ (n=17), Mann-Whitney test, 2-tailed. CCR2 indicates C-C chemokine receptor type 2; H&E, Hematoxylin and Eosin; and LY-6C, lymphocyte antigen 6C.

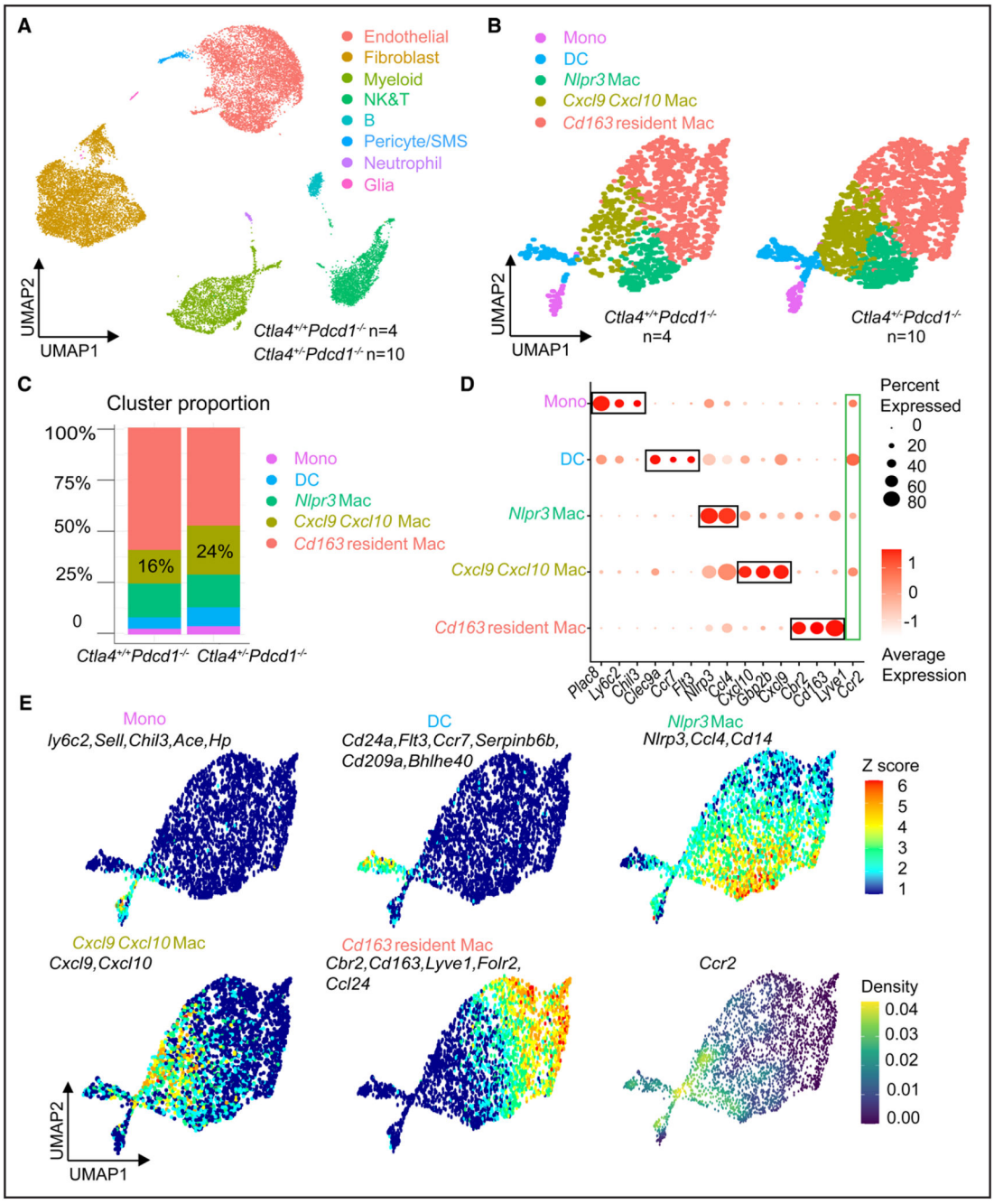

Figure 2. Expansion of *Cxcl9*$^{+}$*Cxcl10*$^{+}$ macrophages in *Ctla4*$^{+/-}$*Pdcd1*$^{-/-}$ mouse hearts.

A, UMAP clustering of 23 606 cells from 14 mouse hearts (*Ctla4*$^{+/+}$*Pdcd1*$^{-/-}$, n=4; *Ctla4*$^{+/-}$*Pdcd1*$^{-/-}$, n=10), showing 8 major cell types. **B**, UMAP clustering of 3209 the myeloid cells spilt by experimental group highlighting 5 transcriptionally distinct subclusters. **C**, The proportion of each myeloid subcluster in *Ctla4*$^{+/+}$*Pdcd1*$^{-/-}$ and *Ctla4*$^{+/-}$*Pdcd1*$^{-/-}$ mice. **D**, Dot plots of differentially expressed genes in each myeloid subcluster. **E**, *Z* score feature plot of enriched genes in each myeloid subcluster and density plot of *Ccr2* expression. Cell state marker genes (black) were selected based on robust enrichment in their respective subclusters. Bhlhe40 indicates basic helix-loop-helix family member e40;

Ccl24, C-C motif chemokine ligand 24; Ccr7, C-C motif chemokine receptor 7; Chil3, Chitinase-like 3; Clec9a, C-type lectin domain containing 9A; DC, dendritic cell; Flt3, fms related receptor tyrosine kinase 3; Mono, monocyte; Plac8, Placenta specific 8; Serpinb6b, serine (or cysteine) peptidase inhibitor, clade B, member 6b; and UMAP, Uniform Manifold Approximation and Projection.

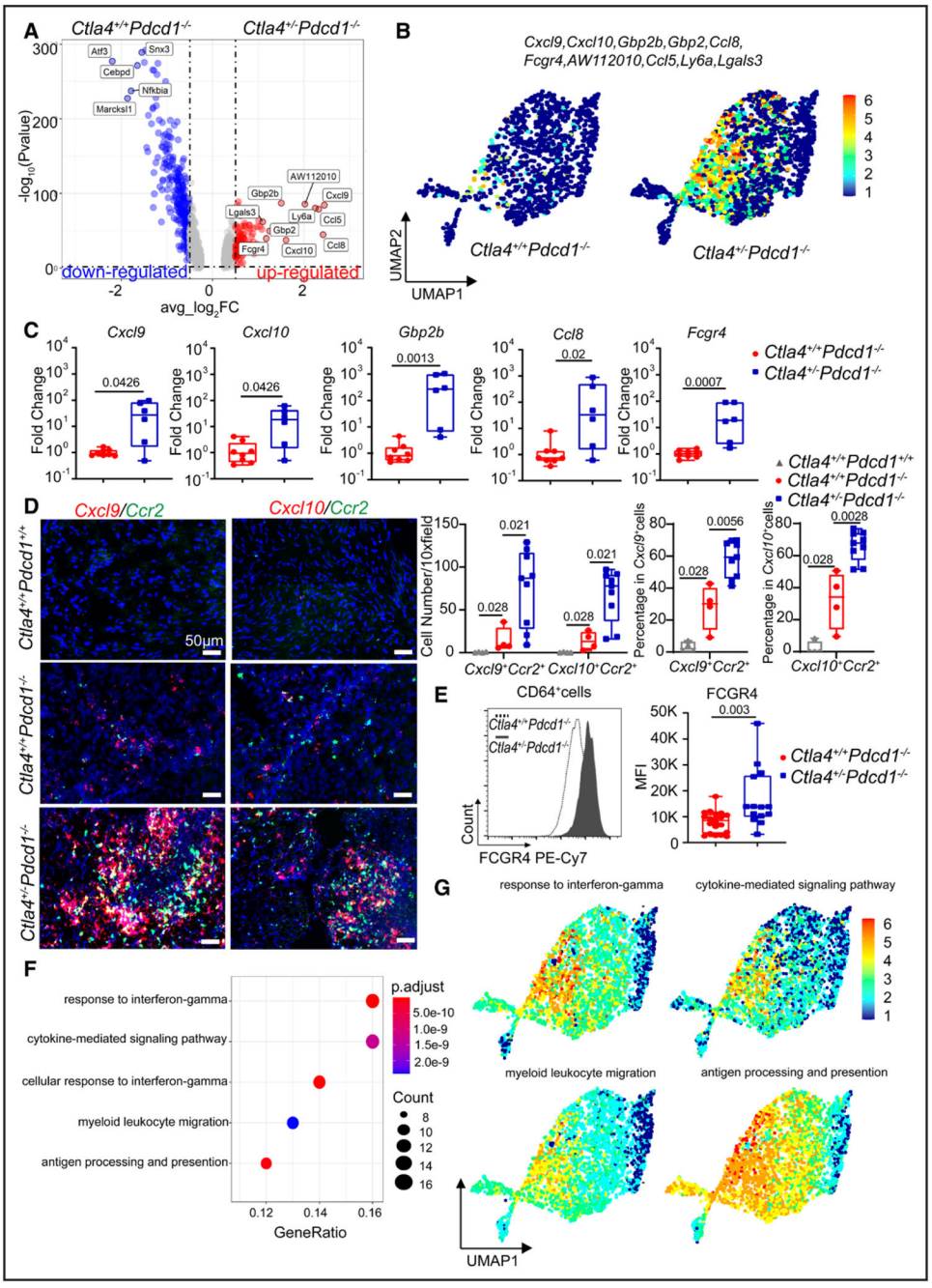

Figure 3. *Cxcl9*$^{+}$*Cxcl10*$^{+}$ macrophages exhibit an activated phenotype in immune checkpoint inhibitor myocarditis.

A, Volcano plot of differentially expressed genes amongst myeloid cells from *Ctla4*$^{+/+}$ *Pdcd1*$^{-/-}$ and *Ctla4*$^{+/-}$*Pdcd1*$^{-/-}$ hearts obtained by Wilcoxon rank-sum test using R package Seurat (v4). **B**, *Z*score feature plot of the top 10 upregulated genes in *Ctla4*$^{+/+}$ *Pdcd1*$^{-/-}$ myeloid cells compared with *Ctla4*$^{+/-}$*Pdcd1*$^{-/-}$ myeloid cells split by experimental group. Differentially expressed genes are selectively expressed in *Cxcl9*$^{+}$*Cxcl10*$^{+}$ macrophages. **C**, Increased *Cxcl9, Cxcl10, Gbp2b, Ccl8,* and *Fcgr4* mRNA expression in *Ctla4*$^{+/+}$ *Pdcd1*$^{-/-}$ compared with *Ctla4*$^{+/-}$*Pdcd1*$^{-/-}$ heart tissue measured by RT-PCR. Data collected from 2

independent experiments, *Ctla4*$^{+/+}$*Pdcd1*$^{-/-}$ (n=8), *Ctla4*$^{+/-}$*Pdcd1*$^{-/-}$ (n=6), Mann-Whitney test, 2-tailed. **D**, Coexpression of *Cxcl9* and *Cxcl10* with *Ccr2* in mouse hearts visualized by RNA in situ hybridization. **Left**, Representative images in each condition; scale bar, 50 μm. **Right**, Quantification of the number of *Cxcl9*$^{+}$*Ccr2*$^{+}$ cells or *Cxcl10*$^{+}$*Ccr2*$^{+}$ cells per 10× field in each condition as well as the percentage of *Cxcl9*$^{+}$*Ccr2*$^{+}$ or *Cxcl10*$^{+}$*Ccr2*$^{+}$ cells in *Cxcl9*$^{+}$ or *Cxcl10*$^{+}$ cells. *Ctla4*$^{+/+}$*Pdcd1*$^{+/+}$ (n=4), *Ctla4*$^{+/+}$*Pdcd1*$^{-/-}$ (n=4), *Ctla4*$^{+/-}$*Pdcd1*$^{-/-}$ (n=9), Mann-Whitney test, 2-tailed. **E**, Quantification of FCGR4 protein expression on CD64^{+} macrophages by flow cytometry. Data collected from 4 independent experiments, *Ctla4*$^{+/+}$*Pdcd1*$^{-/-}$ (n=20), *Ctla4*$^{+/-}$*Pdcd1*$^{-/-}$ (n=14), Mann-Whitney test, 2-tailed. **F**, Gene ontology pathway enrichment analysis of upregulated genes in *Ctla4*$^{+/-}$*Pdcd1*$^{-/-}$ myeloid cells. The top 5 enriched pathways in *Ctla4*$^{+/-}$*Pdcd1*$^{-/-}$ myeloid cells are displayed. Genes used in the analysis were selected from Seurat differential expression with $P < 0.05$ and $\log_2 FC > 0.5$. *P* value calculated using hypergeometric distribution and corrected for multiple comparisons. **G**, *Z* score feature plots of enriched genes involved in response to IFN-γ (interferon gamma), cytokine-mediated signaling pathway, myeloid leukocyte migration, antigen processing, and presentation pathways in myeloid cells. Arf3 indicates ADP ribosylation factor 3; AW112010, expressed sequence AW112010; Ly6a, lymphocyte antigen 6 family member A; Marcksl1, MARCKS like 1; Nfkbia, NFKB inhibitor alpha; and Snx3, sorting nexin 3.

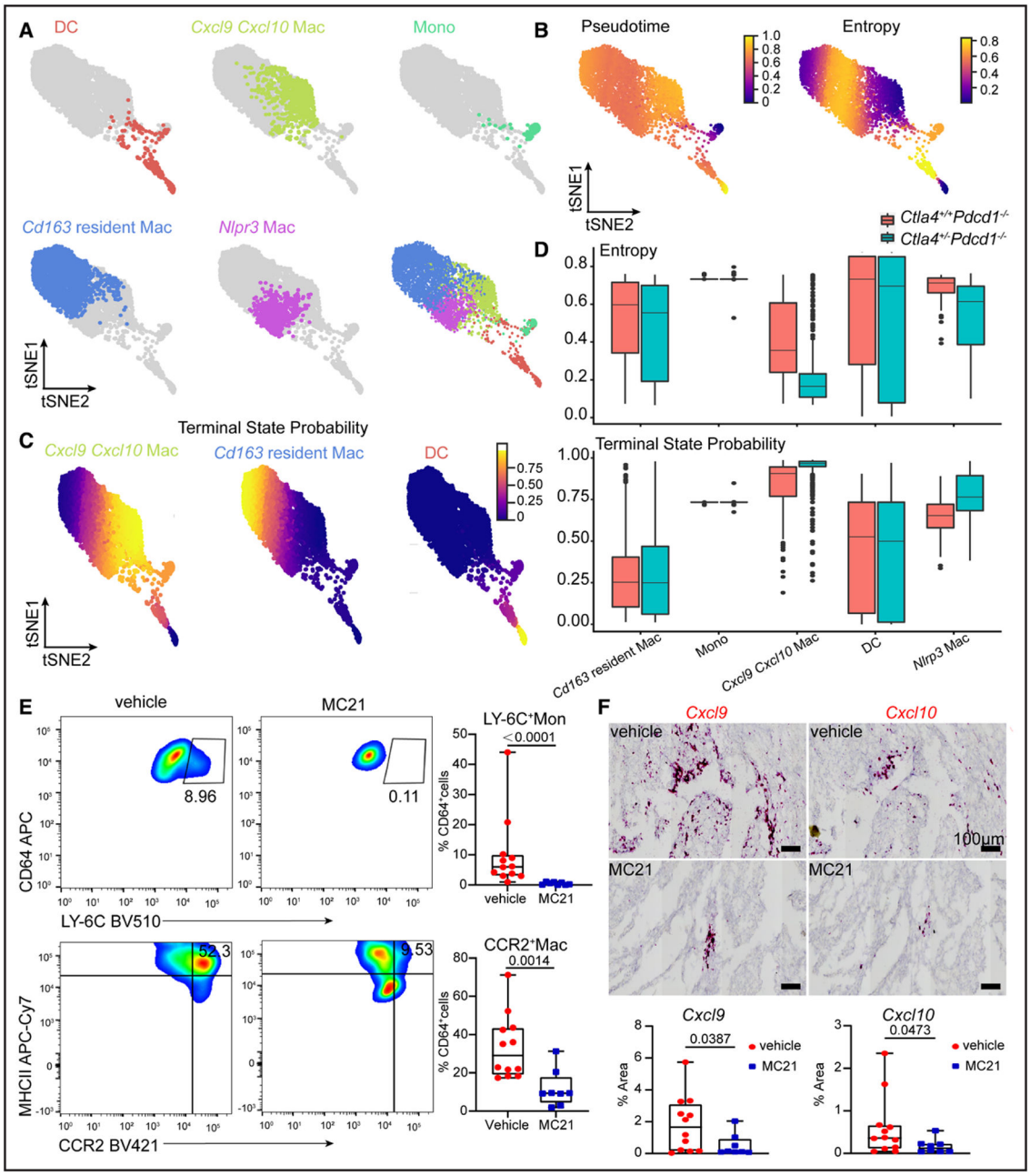

Figure 4. *Cxcl9*$^{+}$*Cxcl10*$^{+}$ macrophages originate from monocytes.

A, tSNE force-directed layout plot of myeloid cells. Cells are colored by cell cluster annotations. **B**, Pseudotime and entropy values of myeloid cells. *Cxcl9*$^{+}$*Cxcl10*$^{+}$ macrophages (*Cxcl9 Cxcl10* Mac) have high pseudotime and low entropy values, suggesting that they represent a differentiated cell state. **C**, Terminal state probability of cell states predicted as differentiated populations: *Cxcl9 Cxcl10* Mac; *Cd163* resident Mac; and DCs. **D**, Box plots of entropy (**upper**) and *Cxcl9 Cxcl10* Mac terminal state probability (**lower**) of myeloid subclusters split by experimental group. **E**, Percentage of LY-6C^{high} monocytes and CCR2^{+} macrophages of cardiac CD64^{+} cells from vehicle or MC-21 antibody-treated mice quantified by flow cytometry. Displayed cells are CD45^{+}LY-6G^{-}CD64^{+}. Data collected

from 4 independent experiments. Vehicle group (n=12), MC-21–treated group (n=8), Mann-Whitney test, 2-tailed. **F**, Representative images (**upper**) and quantification (**lower**) of *Cxcl9* and *Cxcl10* positive cells in the heart 6 days after MC-21 antibody treatment. Data collected from 4 independent experiments. Vehicle group (n=12), MC-21–treated group (n=8), Mann-Whitney test, 2-tailed. DC indicates dendritic cell; and Mono, monocyte.

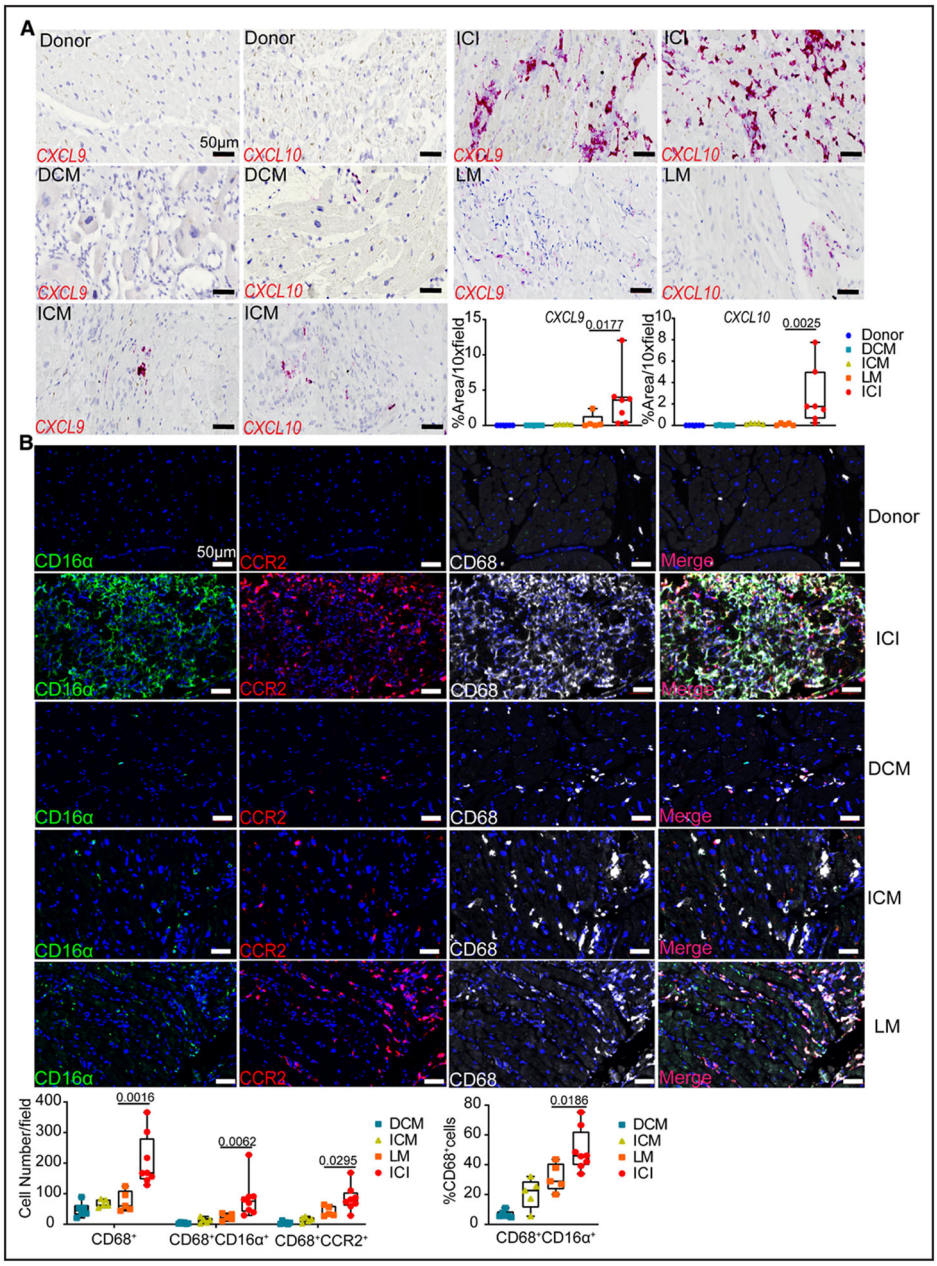

Figure 5. ***CXCL9*$^{+}$*CXCL10*$^{+}$ *macrophages in* human ICI associated myocarditis.**

A, Expression of *CXCL9* and *CXCL10* by RNA in situ hybridization in human heart tissue from patients with immune checkpoint inhibitor myocarditis (ICI, n=7), lymphocytic myocarditis (LM, n=5), ischemic cardiomyopathy (ICM, n=5), or dilated cardiomyopathy (DCM, n=6), and donor control subjects (n=6). Quantification of the number of *CXCL9*$^{+}$ and *CXCL10*$^{+}$ cells, Mann-Whitney test, 2-tailed. Scale bar, 50 μm. **B**, Immunofluorescent staining of CD16α (green), CCR2 (red), CD68 (white), and DAPI (blue) in human heart tissue from patients with ICI (n=8), LM (n=5), ICM (n=5), or DCM (n=6), and donor control subjects (n=6). Quantification of cell number and the percentage of CD68^{+}CD16a^{+} cells in all CD68^{+} cells, Mann-Whitney test, 2-tailed. Scale bar, 50 μm.

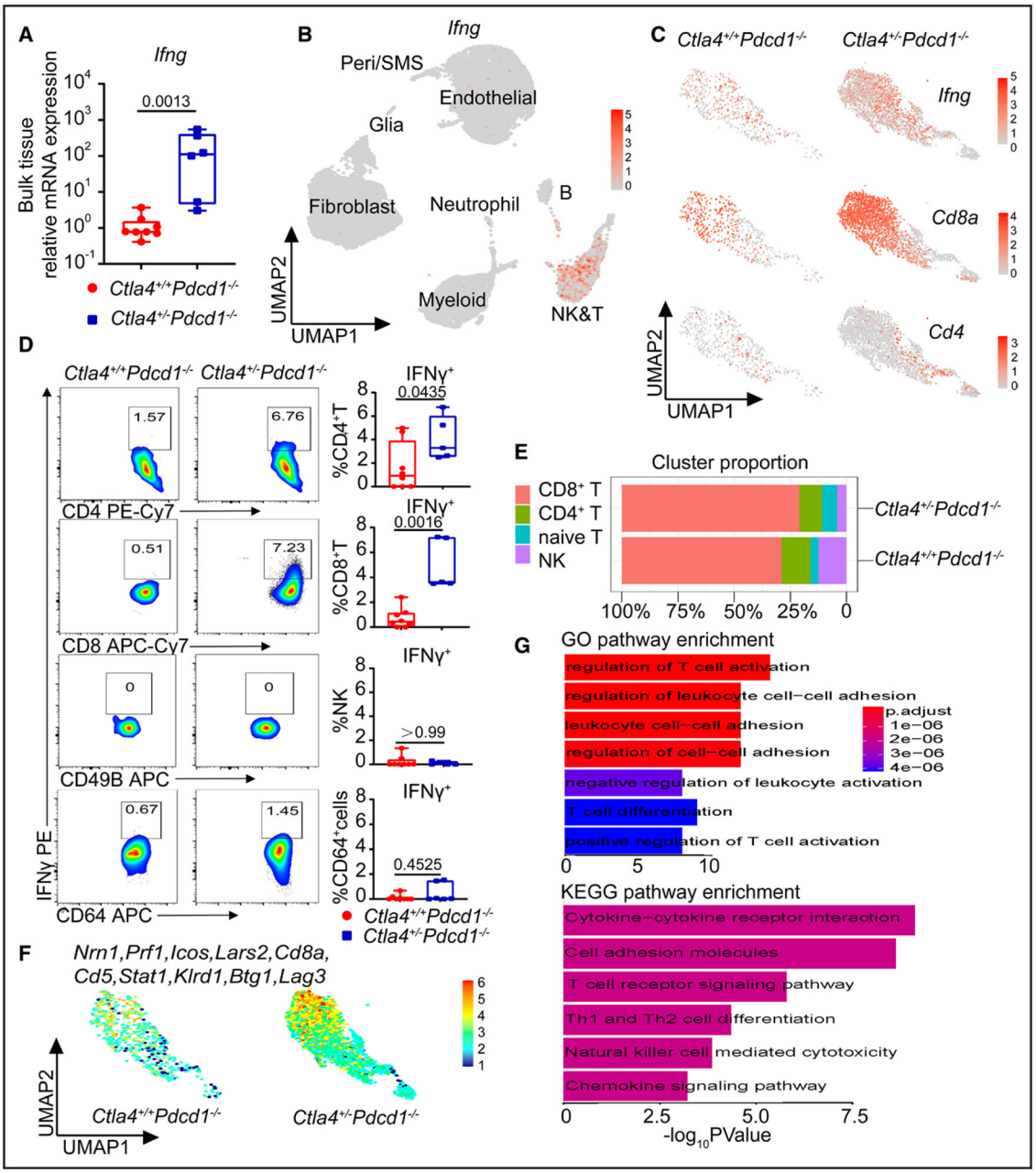

Figure 6. T-cells are the primary source of IFN-γ in immune checkpoint inhibitor myocarditis mouse hearts.

A, Increased *Ifng mRNA* expression in *Ctla-4*$^{+/-}$*Pdcd1*$^{-/-}$ mouse hearts measured by RT-PCR. Data collected from 2 independent experiments, *Ctla4*$^{+/+}$*Pdcd1*$^{-/-}$ (n=8), *Ctla4*$^{+/-}$*Pdcd1*$^{-/-}$ (n=6), Mann-Whitney test, 2-tailed. **B**, Feature plot of *Ifng* expression in all cell types recovered from the heart showing specific expression in the NK/T-cell cluster. **C**, Feature plots of *Ifng, Cd8a,* and *Cd4* expression in NK&T-cells showing CD8 T-cell expansion and enriched *Ifng* expression in CD8 T-cells from *Ctla4*$^{+/-}$*Pdcd1*$^{-/-}$ hearts. **D**, Percentages of IFN-γ^{+}CD4^{+}, IFN-γ^{+}CD8^{+} T-cells, IFN-γ^{+} NK-cells, and IFN-γ^{+}CD64^{+} macrophages analyzed by flow cytometry. Data collected from 2 independent experiments,

Ctla4$^{+/+}$*Pdcd1*$^{-/-}$ (n=8), *Ctla4*$^{+/-}$*Pdcd1*$^{-/-}$ (n=5), Mann-Whitney test, 2-tailed. **E**, The proportion of each NK&T subcluster per experimental group. **F**, *Z* score feature plots of top 10 upregulated genes in *Ctla4*$^{+/-}$*Pdcd1*$^{-/-}$ NK&T-cells compared with *Ctla4*$^{+/+}$*Pdcd1*$^{-/-}$ NK&T cells split by group. **G**, Gene ontology (GO) and Kyoto Encyclopedia of Genes and Genomes (KEGG) enriched pathways using genes upregulated in *Ctla4*$^{+/-}$*Pdcd1*$^{-/-}$ NK&T cells compared with *Ctla4*$^{+/+}$*Pdcd1*$^{-/-}$ NK&T cells. Genes used in the analysis were selected from Seurat differential expression with $P < 0.05$ and $\log_2 FC > 1$. *P* values calculated by hypergeometric distribution using R package ClusterProfiler. Btg1 indicates B-cell translocation gene 1 protein; IFN-γ, interferon gamma; Klrd1, killer cell lectin like receptor D1; Lag3, lymphocyte activating 3; Lars2, probable leucyl-tRNA synthetase, mitochondrial; and Nrn1, neuritin 1.

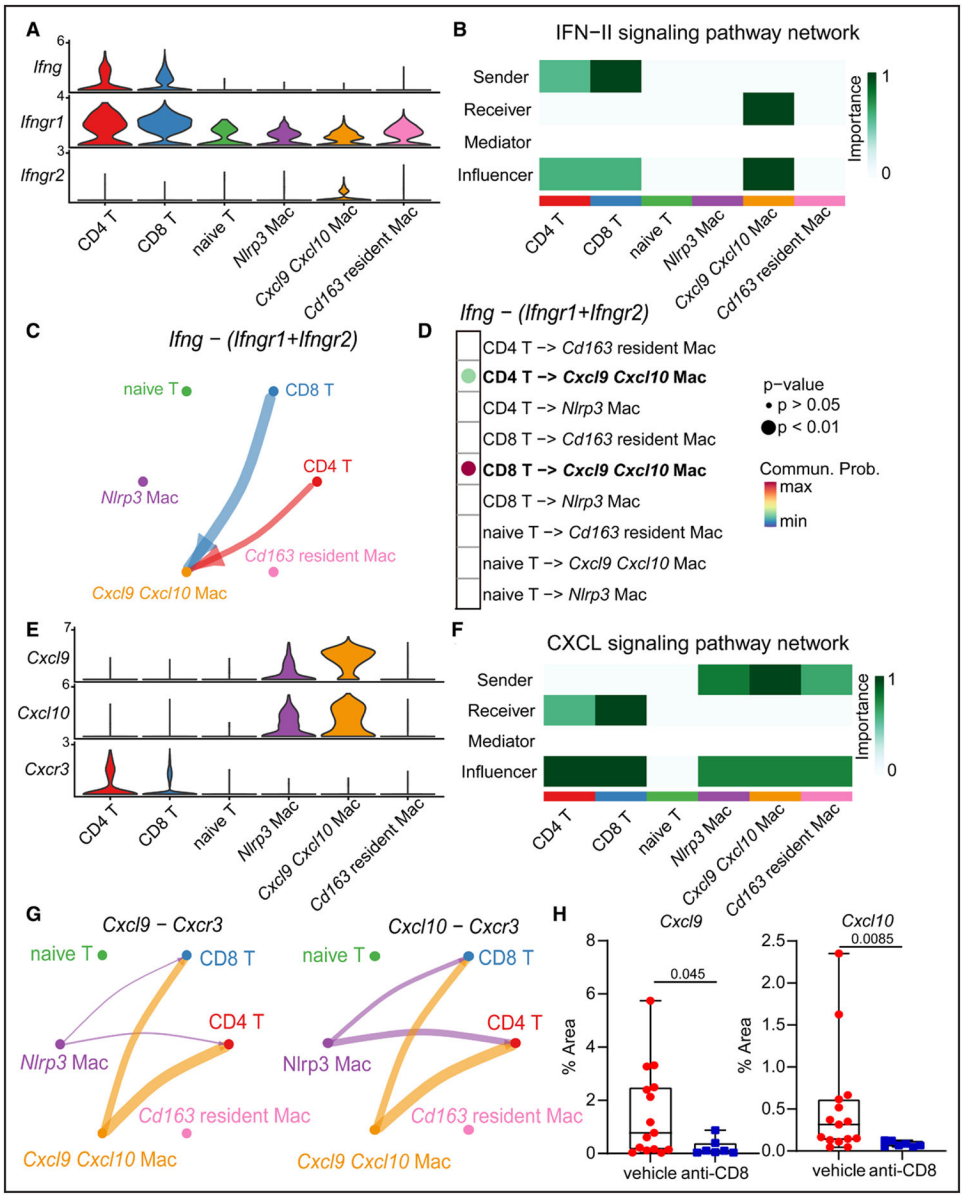

Figure 7. T-cells are predicted to orchestrate the expansion and activation of *Cxcl9*$^{+}$*Cxcl10*$^{+}$ macrophages.

A, Cell to cell communication analysis using CellChat predicted that T-cells signal to macrophages through IFN-γ. Violin plot showing the expression distribution of IFN-γ pathway ligand and receptors in T-cells and macrophages. **B**, Heatmap showing the relative importance of each cell state based on the computed network of IFN-γ signaling. **C**, Circle plot summarizing the inferred intercellular communication network between T-cells and macrophages for IFN-γ signaling. **D**, Dot plot showing the strength of interaction between T-cell and macrophage cell states for IFN-γ signaling. *P* values were calculated using R package CellChat. **E**, Violin plot showing the expression distribution of signaling genes involved in the inferred reciprocal CXCL signaling network (Cxcl9/Cxcl10-Cxcr3) between macrophages and T-cells. **F**, Heatmap displaying the relative importance of each cell state based on the computed network of CXCL signaling. **G**, Circle plot depicting the inferred

intercellular communication network between macrophage and T-cell states for CXCL signaling (Cxcl9/Cxcl10-Cxcr3). **H**, Quantification of cardiac *Cxcl9*$^{+}$ and *Cxcl10*$^{+}$ *cells* 6 days after anti-CD8 antibody treatment. Data collected from 3 independent experiments. Vehicle (n=15), anti-CD8 (n=7), Mann-Whitney test, 2-tailed. Cxcr3 indicates C-X-C motif chemokine receptor 3; Ifng, interferon gamma; and Ifngr, interferon gamma receptor.

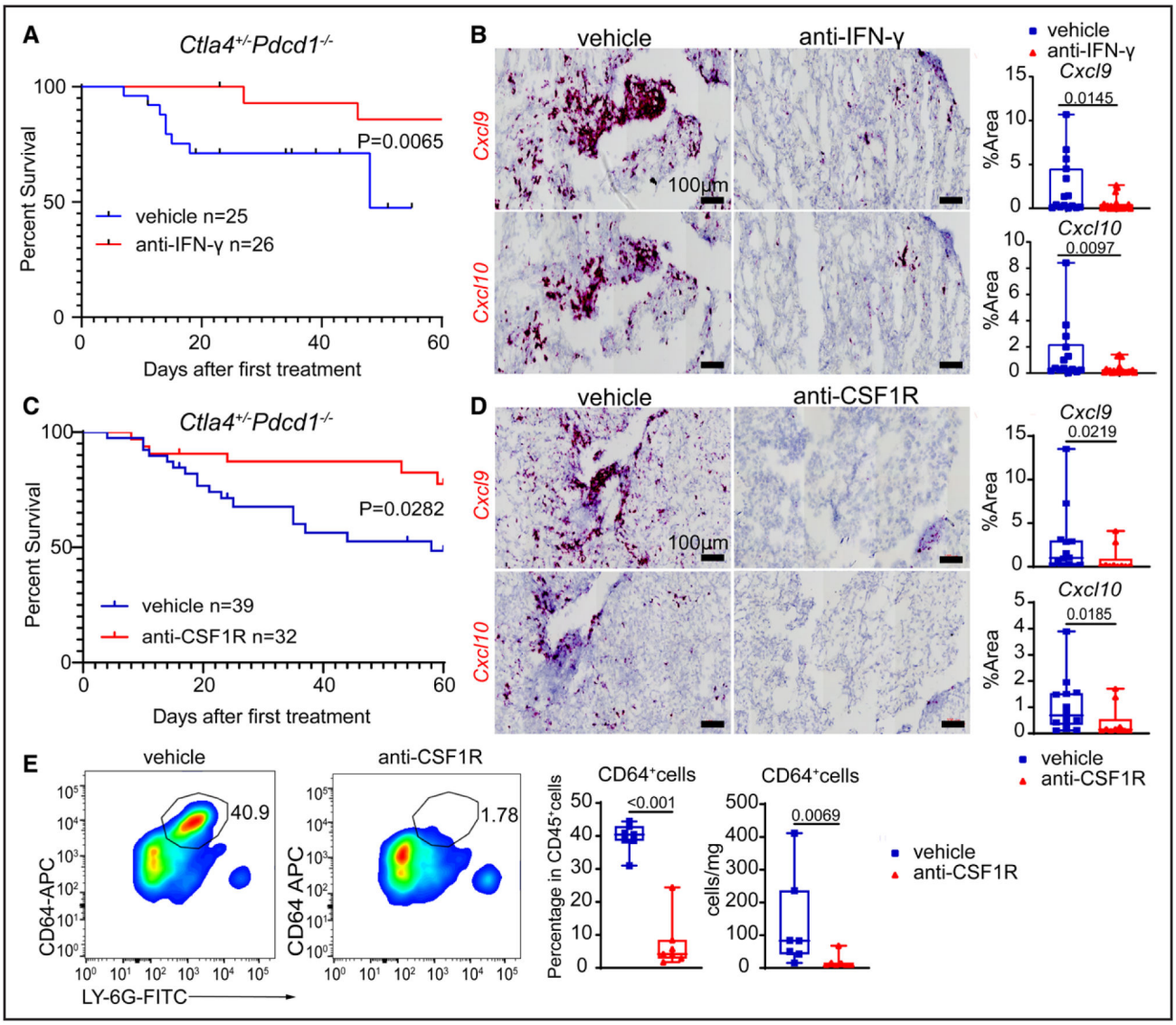

Figure 8. IFN-γ blockade and macrophage depletion reduce cardiac *Cxcl9*$^{+}$*Cxcl10*$^{+}$ macrophages and prolong the survival of *Ctla4*$^{+/-}$*Pdcd1*$^{-/-}$ mice.

A, Survival of Ctla4$^{+/-}$ Pdcd1$^{-/-}$ mice treated with vehicle (isotype control) or anti–IFN-γ antibody (R46A2). Data collected from 4 independent experiments vehicle (n=25); anti–IFN-γ (n=26), log-rank test. **B**, Representative images (**left**) and quantification (**right**) of cardiac *Cxcl9*$^{+}$ and *Cxcl10*$^{+}$ cells as determined by RNA in situ hybridization 23 days after vehicle or anti–IFN-γ antibody treatment. Data collected from 5 independent experiments. Vehicle (n=15), anti–IFN-γ (n=21), Mann-Whitney test, 2-tailed. **C**, Survival of *Ctla4*$^{+/-}$*Pdcd1*$^{-/-}$ mice treated with vehicle (isotype control) or anti-CSF1R antibody (AFS98). Vehicle (n=39), anti-CSF1R (n=32), log-rank test. **D**, Representative images (**left**) and quantification (**right**) of cardiac *Cxcl9*$^{+}$ and *Cxcl10*$^{+}$ cells as determined by RNA in situ hybridization 23 days after vehicle or anti-CSF1R antibody treatment. Data collected from 4 independent experiments. Vehicle (n=14), anti-CSF1R (n=10), Mann-Whitney test, 2-tailed. **E**, Cardiac CD64^{+} macrophages depletion was verified by flow cytometry. Representative

images (**left**) and quantification (**right**) of $CD64^+$ cells as determined by flow cytometry 60 days after first vehicle or anti-CSF1R antibody treatment. Displayed cells (**left**) are gated $CD45^+$ cells. Data collected from 3 independent experiments. Vehicle (n=7), anti-CSF1R (n=7), Mann-Whitney test, 2-tailed. CSR1R indicates colony stimulating factor 1 receptor; IFN-**γ**, interferon gamma; and LY-6G, lymphocyte antigen 6 family member G.